© 2019. Published by The Company of Biologists Ltd | Development (2019) 146, dev183616. doi:10.1242/dev.183616

RESEARCH ARTICLE

The subcortical maternal complex protein Nlrp4f is involved in cytoplasmic lattice formation and organelle distribution

Dandan Qin[1,2,*], Zheng Gao[1,3,*], Yi Xiao[1], Xiaoxin Zhang[1], Haixia Ma[1], Xingjiang Yu[1], Xiaoqing Nie[1,2], Na Fan[4], Xiaoqing Wang[1], Yingchun Ouyang[1], Qing-Yuan Sun[1], Zhaohong Yi[4] and Lei Li[1,2,‡]

ABSTRACT

In mammalian oocytes and embryos, the subcortical maternal complex (SCMC) and cytoplasmic lattices (CPLs) are two closely related structures. Their detailed compositions and functions remain largely unclear. Here, we characterize Nlrp4f as a novel component associated with the SCMC and CPLs. Disruption of maternal Nlrp4f leads to decreased fecundity and delayed preimplantation development in the mouse. Lack of Nlrp4f affects organelle distribution in mouse oocytes and early embryos. Depletion of Nlrp4f disrupts CPL formation but does not affect the interactions of other SCMC proteins. Interestingly, the loss of Khdc3 or Tle6, two other SCMC proteins, also disrupts CPL formation in mouse oocytes. Thus, the absence of CPLs and aberrant distribution of organelles in the oocytes caused by disruption of the examined SCMC genes, including previously reported *Zbed3*, *Nlrp5*, *Ooep* and *Padi6*, indicate that the SCMC is required for CPL formation and organelle distribution. Consistent with the role of the SCMC in CPL formation, the SCMC forms before CPLs during mouse oogenesis. Together, our results suggest that the SCMC protein Nlrp4f is involved in CPL formation and organelle distribution in mouse oocytes.

KEY WORDS: SCMC, NLRP, Organelle, Cytoplasmic lattices, Maternal effect gene, Oocyte-to-embryo transition

INTRODUCTION

Mammalian oocyte-to-embryo transition (OET) comprises numerous specific events, including maternal RNA clearance, organelle rearrangement, epigenetic reprogramming and zygotic genome activation in early embryonic development (Li et al., 2013; Lu et al., 2017). The low transcriptional activity before zygotic genome activation indicates that maternal-effect genes play essential roles in early embryonic development (Li et al., 2013, 2010). Since the initial identification of the maternal-effect genes *Nlrp5* (also known as *Mater*) and *Hsf1* (Christians et al., 2000; Tong et al., 2000), dozens of maternal-effect genes have been reported (Condic, 2016; Li et al., 2010). Yet, how the maternal-effect genes regulate early embryonic development remains poorly understood.

We first described the subcortical maternal complex (SCMC) as a 669-2000 kDa molecular weight complex composed of several proteins encoded by maternal-effect genes; these proteins include Ooep (also known as Floped), Nlrp5, Tle6, Khdc3 (also known as filia) and Zbed3, and plausibly also Nlrp2 and Padi6 (Li et al., 2008; Lu et al., 2017). Based on their direct interactions and roles in the stability of other SCMC proteins, the complex might include three core proteins (Ooep, Nlrp5 and Tle6) (Lu et al., 2017). Depletion of each SCMC core protein leads to decreased expression of other SCMC proteins and results in arrested development at the two-cell stage, suggesting an essential role of this complex in mouse early development and female fertility (Li et al., 2008; Tong et al., 2000; Yu et al., 2014). The SCMC is involved in multiple processes during the mouse OET, including cytoskeleton reorganization, organelle redistribution and cell division (Gao et al., 2018; Lu et al., 2017; Tashiro et al., 2010; Yu et al., 2014). The SCMC genes and this complex might be conserved in other mammals, including humans (Bebbere et al., 2014; Lu et al., 2017; Zhu et al., 2015). Recently, mutations of several human genes encoding the SCMC proteins NLRP5, TLE6, KHDC3L, NLRP2 and PADI6 were reported to be related to human reproductive disorders (Alazami et al., 2015; Docherty et al., 2015; Lu et al., 2017; Mu et al., 2019; Parry et al., 2011; Rezaei et al., 2016). However, details of how the SCMC regulates mammalian embryogenesis and fertility remain unclear.

Several decades ago, cytoplasmic lattices (CPLs), also known as cytoplasmic sheets, paracrystalline arrays, bilaminar lamellae or plaques, were reported to specifically persist in mammalian oocytes and preimplantation embryos (Capco and McGaughey, 1986; Hadek, 1966; Weakley, 1966; Zamboni, 1970). CPL fibers are absent in primary oocytes, gradually appear as oocytes grow, become abundant in fully grown oocytes and persist until the blastocyst stage (Gallicano et al., 1991; Wassarman and Josefowicz, 1978; Yurttas et al., 2008; Zamboni, 1970). CPLs undergo large spatial rearrangements during fertilization, embryo compaction and blastocyst formation (Capco and McGaughey, 1986; Gallicano et al., 1991). CPLs might be the specific structure of the cytoskeleton, including intermediate filaments or other unknown components (Capco et al., 1993; Gallicano et al., 1994). Padi6, also known as ePAD, is the first oocyte-specific protein identified to localize to CPLs in the mouse (Wright et al., 2003). Genetic depletion of *Padi6* results in the absence of CPLs, arrested development at the two-cell stage and female infertility (Esposito et al., 2007). Padi6 is reported to associate with Nlrp5 or Ooep (two SCMC proteins), which have been shown to localize to CPLs in mouse oocytes (Kim et al., 2010; Tashiro et al., 2010). CPLs are absent in oocytes from *Ooep* and *Nlrp5* null females (Kim et al., 2010; Tashiro et al., 2010). These results suggest a close relationship between the SCMC and CPLs.

NLRP subfamily proteins, containing an N-terminal pyrin domain (PYD), a NACHT nucleotide-binding domain and

[1]State Key Laboratory of Stem Cell and Reproductive Biology, Institute of Zoology, Chinese Academy of Sciences, Beijing, 100101, China. [2]University of Chinese Academy of Sciences, Beijing, 100049, China. [3]Reproductive Medicine Center of the Third Affiliated Hospital of Guangzhou Medical University, Guangzhou, 510150, China. [4]Key Laboratory of Urban Agriculture (North) of Ministry of Agriculture, College of Biological Science and Engineering, Beijing University of Agriculture, Beijing, 102206, China.
*These authors contributed equally to this work

[‡]Author for correspondence (lil@ioz.ac.cn)

Q.-Y.S., 0000-0002-0148-2414; L.L., 0000-0001-5478-5681

Received 12 August 2019; Accepted 13 September 2019

Development (2019) 146, dev183616. doi:10.1242/dev.183616

C-terminal leucine-rich repeats (LRRs), are well known for their roles in innate immunity, where they participate in the assembly of inflammasomes (Martinon et al., 2007; Ratsimandresey et al., 2013; Zambetti et al., 2012). These subfamily proteins also play important roles in female reproduction in mammals (Kuchmiy et al., 2016; Mahadevan et al., 2017; Monk et al., 2017; Murdoch et al., 2006; Tong et al., 2000). *Nlrp4f* was initially identified as an oocyte-specific gene similar to *Nlrp5* in the mouse (Dadé et al., 2004). Later, *Nlrp4f* was identified as one of the downstream targets of Figla, an oocyte-specific transcription factor (Joshi et al., 2007). However, the physiological function of Nlrp4f remains unknown. Here, we characterized Nlrp4f as a novel component associated with the SCMC and CPLs. Genetic ablation of *Nlrp4f* showed that maternal Nlrp4f is required for mouse preimplantation development and female fertility. Furthermore, investigation of the relationship between the SCMC and CPLs using SCMC mutants indicated that the SCMC is involved in CPL formation.

RESULTS

Identification of Nlrp4f as a novel component of the SCMC

CPLs are resistant to Triton X-100 extraction and are absent in *Nlrp5* null oocytes (Gallicano et al., 1991; Kim et al., 2010). Using *Nlrp5* null oocytes as a negative control, we extracted mouse oocytes with Triton X-100 to identify new components of CPLs (see Materials and Methods). The insoluble and soluble fractions were separated by SDS-PAGE and stained with Coomassie Brilliant Blue (Fig. 1A). Two protein bands (1 and 2) were found in the insoluble fraction of $Nlrp5^{+/+}$ and $Nlrp5^{+/-}$ but not $Nlrp5^{-/-}$ oocytes and were analyzed

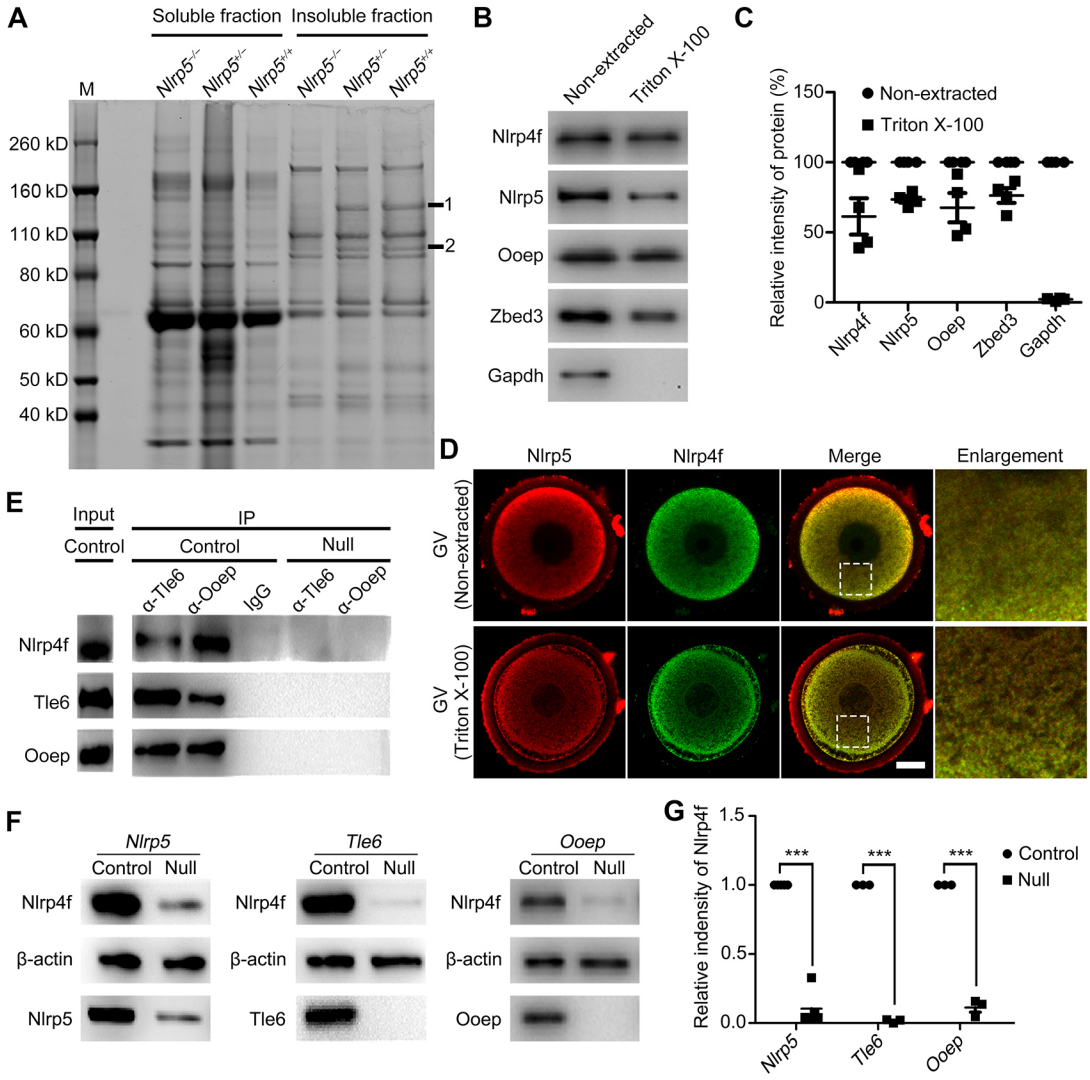

Fig. 1. Identification of Nlrp4f as a novel component of the SCMC. (A) GV oocytes from $Nlrp5^{+/+}$, $Nlrp5^{+/-}$ and $Nlrp5^{-/-}$ females were extracted with buffer containing Triton X-100. The soluble and insoluble fractions were separated by SDS-PAGE and stained with Coomassie Brilliant Blue. Bands 1 and 2 indicate the proteins in $Nlrp5^{+/+}$ and $Nlrp5^{+/-}$ oocytes but not in $Nlrp5^{-/-}$ oocytes. (B) Normal mouse GV oocytes were treated with extraction buffer, followed by immunoblotting with specific antibodies for the SCMC proteins. (C) Quantification of protein band intensities in B. Four independent experiments were performed. (D) GV oocytes were isolated from normal females and left untreated or treated with extraction buffer. Oocytes were stained with anti-Nlrp5 (red) and anti-Nlrp4f antibodies (green). Scale bar: 20 µm. (E) Normal ovarian lysates were precipitated with anti-Tle6 and anti-Ooep antibodies or IgG (negative control). The precipitates produced were examined by immunoblot using specific antibodies for Nlrp4f, Tle6 and Ooep. Ovarian lysates from *Tle6* or *Ooep* null mice were also used as negative controls. (F) GV oocytes were isolated from normal control, $Nlrp5^{-/-}$, $Tle6^{-/-}$and $Ooep^{-/-}$ females. The levels of SCMC proteins were examined by immunoblot with specific antibodies. β-actin was used as the loading control. (G) Quantification of Nlrp4f band intensity in *Nlrp5*, *Tle6* and *Ooep* null GV oocytes in F. Error bars indicate s.e.m., ***P<0.001.

Development (2019) 146, dev183616. doi:10.1242/dev.183616

by tandem mass spectrometry (Fig. 1A). We identified Nlrp5 with 45 peptides as the primary protein in band 1, and Nlrp4f with 33 peptides in band 2 as a novel component associated with CPLs. To confirm the mass spectrometry results, we extracted normal mouse germinal vesicle (GV) stage oocytes with Triton X-100 and examined the insoluble fraction by western blot for Nlrp4f and other known CPL-associated proteins, including Nlrp5, Ooep and Zbed3. Similar to the other related proteins of CPLs, Nlrp4f was resistant to Triton X-100 extraction (Fig. 1B,C). These data suggest that Nlrp4f is a novel component associated with CPLs.

Using mouse anti-Tle6 antibody to precipitate the lysates of mouse oocytes, combined with mass spectrometry, we previously identified 23 potential SCMC proteins including Tle6, Nlrp5, Ooep, Khdc3 and Zbed3 (Gao et al., 2018), as well as Nlrp4f with 14 peptides (Fig. S1). Immunostaining showed that Nlrp4f colocalized with the SCMC protein Nlrp5 in the subcortex and cytoplasm of mouse oocytes, especially after extraction (Fig. 1D). Co-immunoprecipitation (Co-IP) showed that both Tle6 and Ooep antibodies specifically precipitated Nlrp4f, as well as Ooep and Tle6, in normal mouse ovarian lysates (Fig. 1E). Similar to the decreased level of SCMC proteins (Gao et al., 2018; Li et al., 2008; Yu et al., 2014), Nlrp4f was also decreased in the oocytes with disruption of SCMC core proteins Nlrp5, Tle6 or Ooep (Fig. 1F,G). These results identify Nlrp4f as a novel component of the SCMC in mouse oocytes.

Nlrp4f is specifically expressed in mouse oocytes and early embryos

Quantitative reverse transcription PCR (qRT-PCR) showed that *Nlrp4f* mRNA was highly expressed in mouse ovaries (Fig. 2A). Compared with fully grown oocytes, *Nlrp4f* mRNA persisted at high levels in one-cell stage embryos but decreased in two-cell stage embryos (Fig. 2B). Western blots showed that Nlrp4f was primarily detected in mouse ovaries, but not in other tissues (Fig. 2C). In mouse oocytes and preimplantation embryos, Nlrp4f protein remained at high levels until the morula stage (Fig. 2D). Immunofluorescence showed that Nlrp4f protein was localized in the cytoplasm of oocytes and preimplantation embryos, and concentrated at their subcortex (Fig. 2E).These data suggest that *Nlrp4f* is specifically expressed in oocytes and early embryos in the mouse.

Nlrp4f plays an important role in mouse female fertility

To investigate the role of Nlrp4f, we generated *Nlrp4f* knockout mice by targeting its exon 2 using CRISPR/Cas9 technology (Fig. S2A). DNA sequencing showed that a male founder was

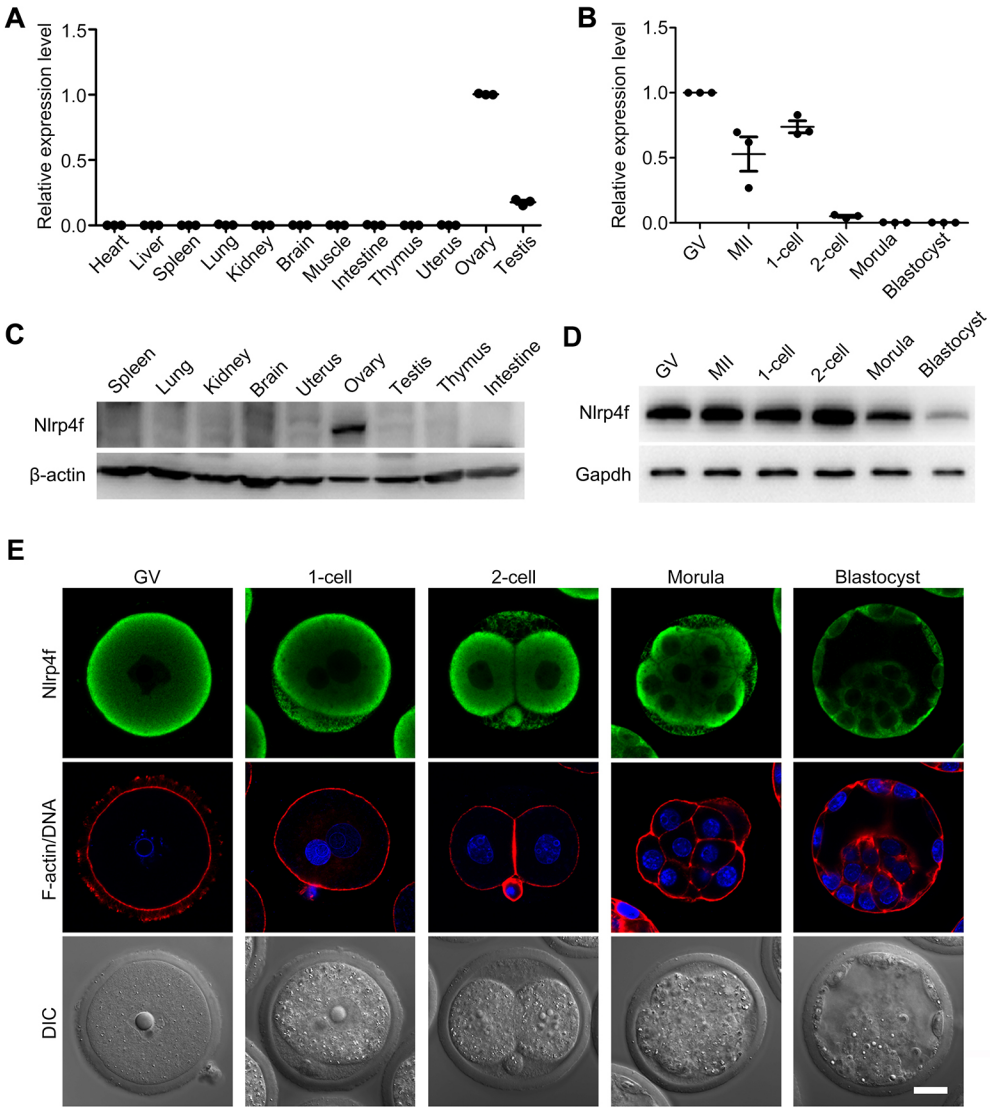

Fig. 2. Expression patterns of *Nlrp4f* in the mouse. (A) *Nlrp4f* mRNA levels were determined by qRT-PCR in heart, liver, spleen, lung, kidney, brain, muscle, intestine, thymus, uterus, ovary and testis of adult mice. The level of *Nlrp4f* mRNA expression in the ovary was set as 1. (B) qRT-PCR analysis of *Nlrp4f* mRNA expression in GV, MII oocytes, one-cell, two-cell, morula and blastocyst embryos. The level of *Nlrp4f* mRNA expression in GV oocytes was set as 1. (C) Tissue lysates from mice at postnatal day 10 (P10) were examined by immunoblot with specific antibodies for Nlrp4f and β-actin (loading control). (D) Protiens were detected by immunoblot with specific antibodies for Nlrp4f and Gapdh (loading control) in oocytes and preimplantation embryos from normal females. (E) GV oocytes and preimplantation embryos were stained with anti-Nlrp4f antibody, Alexa Fluor 546 phalloidin (F-actin) and Hochest 33342 (DNA). Scale bar: 20 µm.

Development (2019) 146, dev183616. doi:10.1242/dev.183616

obtained with a mutation at the *Nlrp4f* gene locus (Fig. S2A). This founder was used to establish the *Nlrp4f* mutant mouse line. *Nlrp4f*$^{-/-}$ mice grew into adults and appeared mostly normal. The results of qRT-PCR revealed that *Nlrp4f* mRNA was absent in oocytes from *Nlrp4f*$^{-/-}$ females (Fig. S2B). Western blots and immunostaining confirmed the successful ablation of Nlrp4f protein in oocytes from *Nlrp4f*$^{-/-}$ females (Fig. S2C,D).

We then examined fertility by mating. *Nlrp4f*$^{-/-}$ males exhibited normal fertility after mating for three months (Fig. 3A). However, compared with *Nlrp4f*$^{+/+}$ females, *Nlrp4f*$^{-/-}$ female mice produced fewer pups (Fig. 3A). We then performed Hematoxylin and Eosin (H&E) staining for *Nlrp4f*$^{+/+}$ and *Nlrp4f*$^{-/-}$ ovaries. The results showed that primordial, growing and mature follicles, as well as corpora lutea (CL), were present in both *Nlrp4f*$^{+/+}$ and *Nlrp4f*$^{-/-}$ ovaries (Fig. 3B). We also examined the ratio of nonsurrounded nucleolus (NSN)-type and surrounded nucleolus (SN)-type fully grown oocytes from *Nlrp4f*$^{+/+}$ and *Nlrp4f*$^{-/-}$ ovaries. Compared with controls, the ratio of NSN or SN oocytes from *Nlrp4f*$^{-/-}$ females did not change significantly (Fig. S3A,B). Furthermore, similar numbers of metaphase II (MII) oocytes were recovered from *Nlrp4f*$^{+/+}$ and *Nlrp4f*$^{-/-}$ females after superovulation with gonadotrophins (Fig. S4A,B). This suggests that Nlrp4f plays a role in female fertility, but is not essential for mouse ovulation or male fertility.

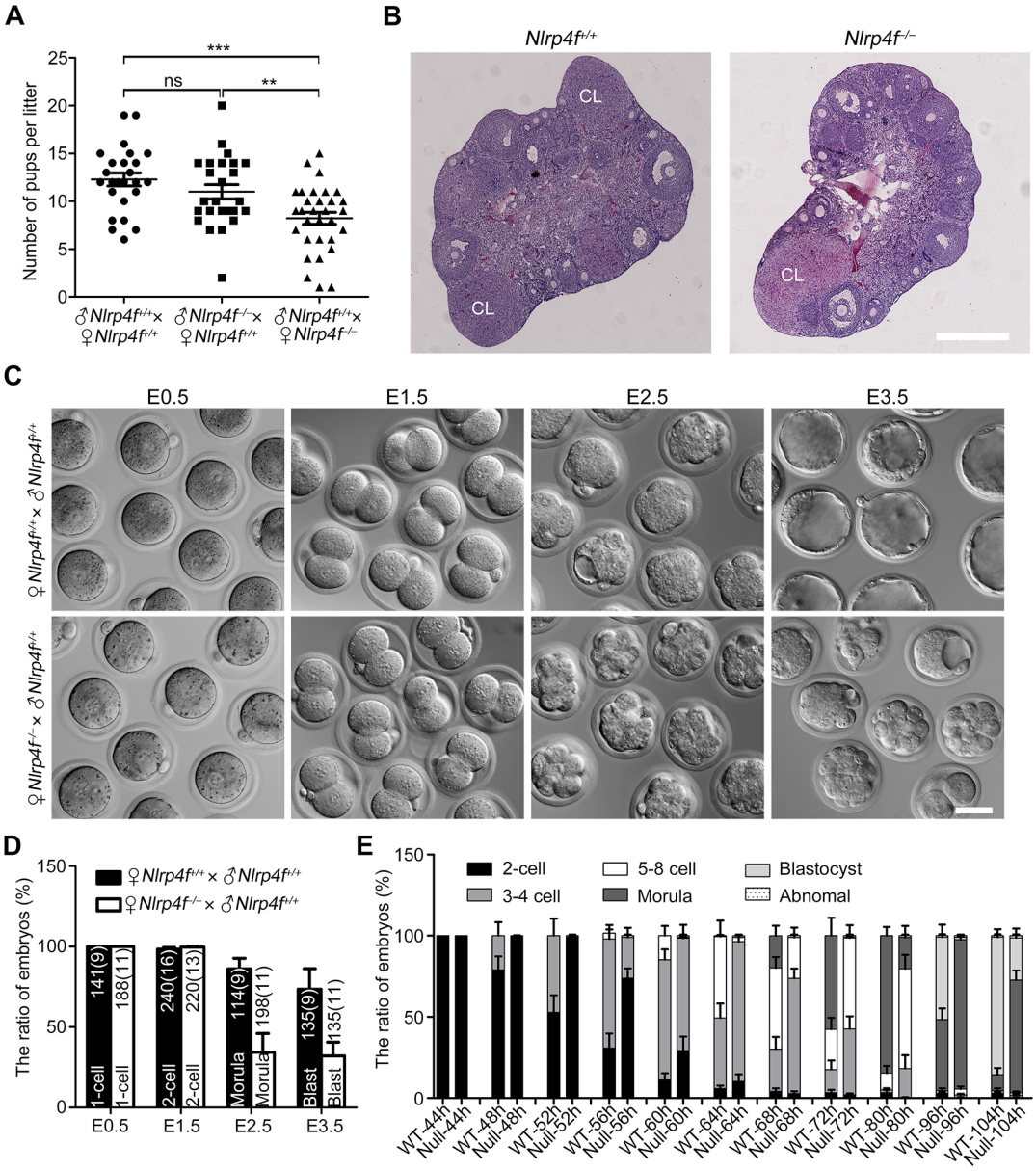

Fig. 3. Depletion of Nlrp4f impairs female fertility and preimplantation development. (A) *Nlrp4f*$^{+/+}$ (wild type) and *Nlrp4f*$^{-/-}$ males were mated with *Nlrp4f*$^{+/+}$ and *Nlrp4f*$^{-/-}$ females for three successive months. The litter sizes were recorded. (B) H&E staining of ovarian sections from two-month-old *Nlrp4f*$^{+/+}$ and *Nlrp4f*$^{-/-}$ females. CL, corpus luteum. (C) Representative images of the bright field of embryos flushed from control and *Nlrp4f*$^{-/-}$ females at E0.5, E1.5, E2.5 and E3.5. (D) Quantification of *in vivo* preimplantation embryos (one-cell, two-cell, morulae and blastocysts) after collection from *Nlrp4f*$^{+/+}$ and *Nlrp4f*$^{-/-}$ females at specific time points. The numbers in the graph reflected the number of analyzed embryos (number of females). Blast, blastocyst. (E) Two-cell embryos (234 from 16 *Nlrp4f*$^{+/+}$ females and 219 from 13 *Nlrp4f*$^{-/-}$ females in three independent experiments) were cultured *in vitro* for 60 h. Embryonic progression of different stages was morphologically assessed every 4 h. The data represent the ratio of different stage embryos at 4 h intervals. Error bars indicate s.e.m. **P<0.01, ***P<0.001; ns, not significant. Scale bars: 500 µm (B); 50 µm (C).

Development (2019) 146, dev183616. doi:10.1242/dev.183616

Nlrp4f is required for mouse preimplantation development

Next, we isolated preimplantation embryos from *Nlrp4f*$^{+/+}$ *and* *Nlrp4f*$^{-/-}$ females after mating with normal males. Similar numbers of one- and two-cell stage embryos were recovered from *Nlrp4f*$^{+/+}$ and *Nlrp4f*$^{-/-}$ females at embryonic day (E)0.5 and E1.5 (Fig. 3C,D). The loss of maternal Nlrp4f had mininal effect on the total numbers of embryos at E2.5 and E3.5 (Fig. 3D). However, the majority of embryos from *Nlrp4f*$^{-/-}$ females displayed a delay in embryo compaction and blastocyst cavitation (Fig. 3C,D; Fig. S5). We also isolated two-cell embryos from normal and *Nlrp4f*$^{-/-}$ females after treatment with gonadotrophins and cultured these embryos *in vitro* for 60 h. The cultured embryos also displayed similar developmental delays (Fig. 3E). Thus, Nlrp4f is required for mouse preimplantation development.

Nlrp4f is involved in organelle distribution in oocytes and embryos

The distribution of organelles such as endoplasmic reticulum (ER) and mitochondria is linked to early embryo and female fertility (Fernandes et al., 2012; Gao et al., 2018). Thus, we examined organelle distribution in zygotes from *Nlrp4f*$^{+/+}$ and *Nlrp4f*$^{-/-}$ females using ER-Tracker and MitoTracker to label the ER and mitochondria, respectively. In control zygotes from *Nlrp4f*$^{+/+}$ females, the ER and mitochondria were concentrated around the male and female pronucleus during interphase and aggregated around the mitotic spindle following nuclear envelope break down (NEBD) (Fig. 4A). However, in zygotes from *Nlrp4f*$^{-/-}$ females, the ER and mitochondria were concentrated around male and female pronucleus, and also aggregated in the subcortical region (Fig. 4A). Live imaging using MitoTracker confirmed that depletion of Nlrp4f led to the disorganized distribution of mitochondria in the zygote (Fig. 4B; Movies 1 and 2).

We also examined the distribution of ER and mitochondria in oocytes from *Nlrp4f*$^{+/+}$ and *Nlrp4f*$^{-/-}$ females. Here, the organelles radially distributed around the nucleus at GV, around the spindles after germinal vesicle break down (GVBD), and also around the spindles at MII oocytes (Fig. 4C). However, in *Nlrp4f*$^{-/-}$ oocytes, they localized around both the nucleus and cortical region at the GV

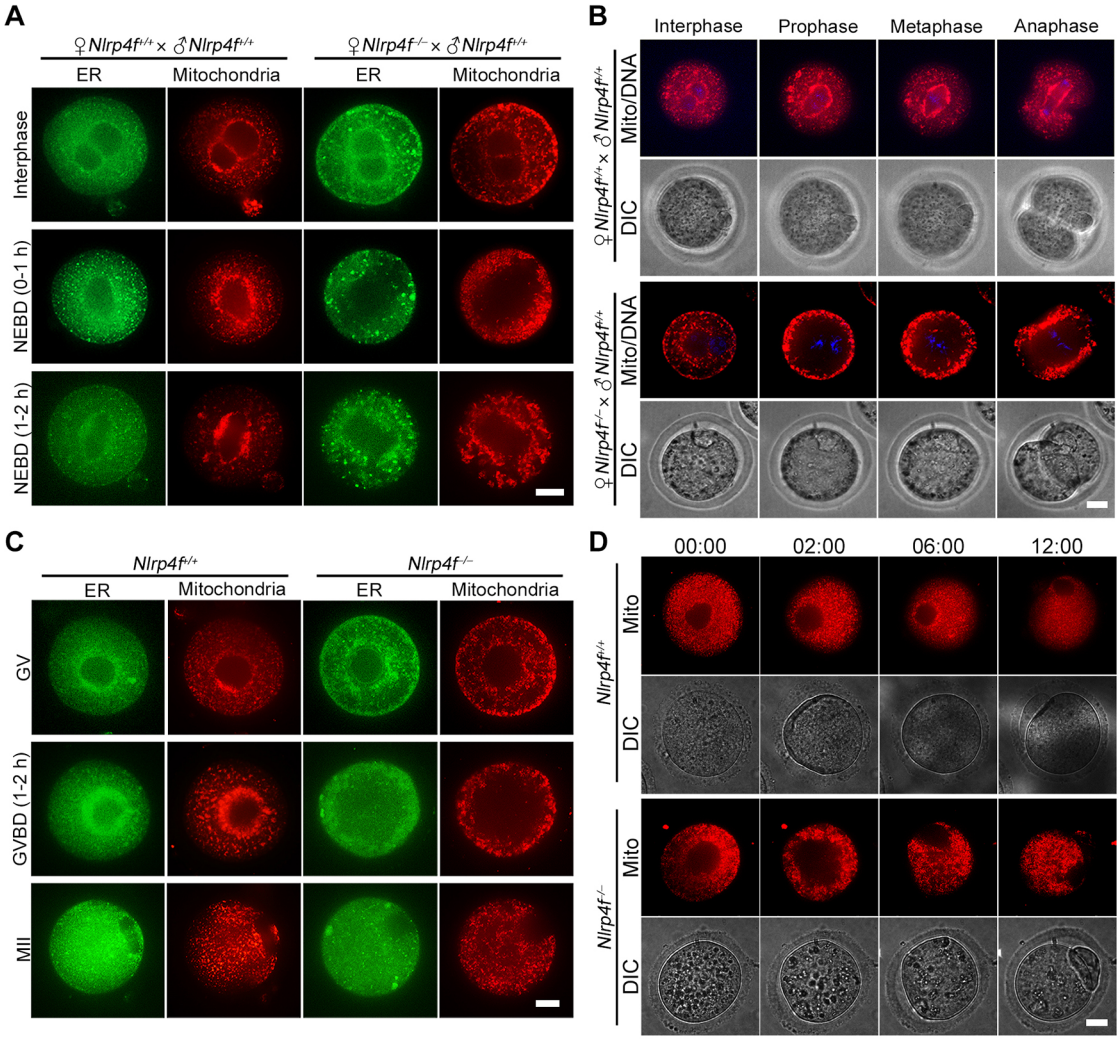

Fig. 4. Disordered organelle distribution in zygotes and oocytes with depletion of Nlrp4f. (A) Zygotes were isolated from *Nlrp4f*$^{+/+}$ (control) and *Nlrp4f*$^{-/-}$ (null) females after mating with normal fertile males. ER and mitochondria were labeled with ER-Tracker (green) and MitoTracker (red), respectively. Control (interphase, *n*=29; NEBD 0-1 h, *n*=27; NEBD 1-2 h, *n*=15) and Nlrp4f null (interphase, *n*=38; NEBD 0-1 h, *n*=22; NEBD 1-2 h, *n*=22) zygotes were examined in three independent experiments. (B) Zygotes from *Nlrp4f*$^{+/+}$ (control) and *Nlrp4f*$^{-/-}$ (Nlrp4f null) females were labeled with MitoTracker (red) for mitochondria and Hoechst 33342 (blue) for DNA. Live imaging of embryos was performed with UltraVIEW-VoX. The stages of embryos were determined by DNA staining and morphology. (C) Oocytes were isolated from *Nlrp4f*$^{+/+}$ (control) and *Nlrp4f*$^{-/-}$ (null) females and were labeled with ER-Tracker (green) and MitoTracker (red) for ERs and mitochondria, respectively. Control (GV, *n*=14; GVBD 1-2 h, *n*=40; MII, *n*=68) and null (GV, *n*=33; GVBD 1-2 h, *n*=77; MII, *n*=74) oocytes were investigated in four independent experiments. (D) Live imaging of the maturation of oocytes after labeling with MitoTracker for mitochondria. Scale bars: 20 µm.

Development (2019) 146, dev183616. doi:10.1242/dev.183616

stage, became concentrated in the subcortical region after GVBD and were dispersed throughout the cytoplasm at the MII stage (Fig. 4C). Live imaging confirmed that depletion of Nlrp4f resulted in defective mitochondrial distribution during mouse oocyte maturation (Fig. 4D; Movies 3 and 4). These data suggest that Nlrp4f is involved in organelle distribution or redistribution during mouse oocyte maturation and zygote development.

Nlrp4f is required for CPL formation in mouse oocytes

Microtubules (MT) and acetylated tubulin are involved in organelle redistribution during mouse oocyte maturation (Gao et al., 2018; Kan et al., 2011). Thus, we examined the expression of acetylated tubulin in *Nlrp4f*$^{-/-}$ oocytes using western blotting. This revealed a decrease in acetylated α-tubulin in *Nlrp4f*$^{-/-}$ GV and MII oocytes (Fig. 5A). Treatment with the deacetylase inhibitor trichostatin A (TSA) significantly increased the level of acetylated α-tubulin in oocytes from both *Nlrp4f*$^{+/+}$ and *Nlrp4f*$^{-/-}$ females (Fig. 5B; Fig. S6A). However, TSA treatment did not rescue the disorganized distribution of organelles in *Nlrp4f*$^{-/-}$ oocytes (Fig. 5C). Immunostaining showed that spindle MTs formed in both *Nlrp4f*$^{-/-}$ and control oocytes after GVBD, but the astral-like MTs were longer in *Nlrp4f*$^{-/-}$ oocytes than those in *Nlrp4f*$^{+/+}$ oocytes following GVBD (Fig. 5D). However, nocodazole treatment did not dramatically affect the subcortical distribution of organelles in 64% (30/47) of *Nlrp4f*$^{-/-}$ oocytes after GVBD (Fig. 5E; Fig. S6B), suggesting that the lengthened microtubules are not the predominant cause of organelle localization to the subcortex in *Nlrp4f*$^{-/-}$ oocytes.

As CPLs might also be associated with organelle distribution in oocytes (Gao et al., 2018; Kan et al., 2011), we investigated CPLs in the ovaries of *Nlrp4f*$^{+/+}$ and *Nlrp4f*$^{-/-}$ females using transmission electron microscopy (TEM). As expected, CPLs were abundant in control oocytes from *Nlrp4f*$^{+/+}$ ovaries (Fig. 5F). However, CPLs were largely absent in oocytes from *Nlrp4f*$^{-/-}$ ovaries (Fig. 5F), suggesting that Nlrp4f is required for CPL formation.

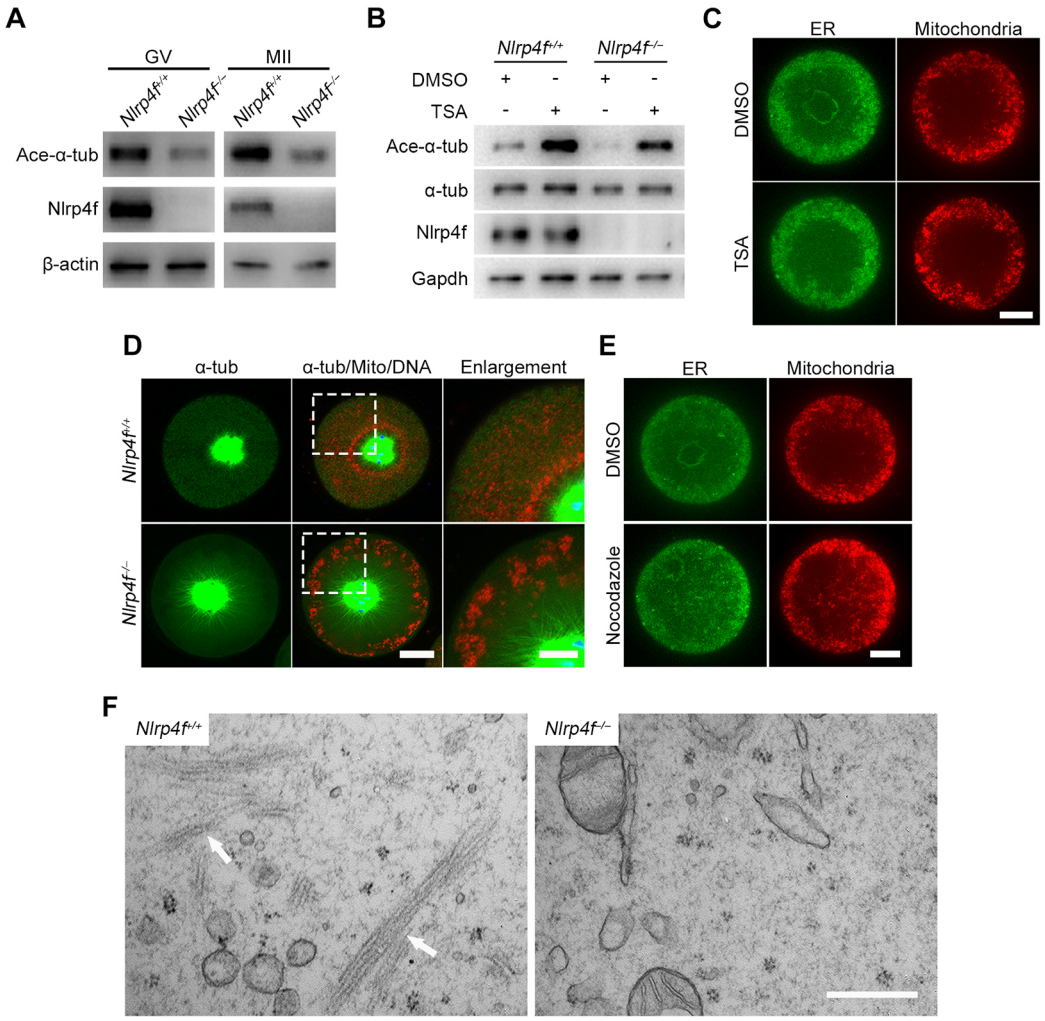

Fig. 5. Abnormal formation of microtubules and CPLs in *Nlrp4f*$^{-/-}$ oocytes. (A) Immunoblot of acetylated α-tubulin, Nlrp4f and β-actin in GV and MII oocytes from *Nlrp4f*$^{+/+}$ and *Nlrp4f*$^{-/-}$ females. (B) GV oocytes were isolated from *Nlrp4f*$^{+/+}$ and *Nlrp4f*$^{-/-}$ females and treated with DMSO and TSA. Immunoblot was performed for these oocytes at GVBD 1-2 h with the antibodies for acetylated α-tubulin, α-tubulin, Nlrp4f, and Gapdh. (C) ER and mitochondria were labeled with ER-Tracker (green) and MitoTracker (red) in *Nlrp4f*$^{-/-}$ oocytes treated with DMSO and TSA after GVBD (1-2 h). (D) *Nlrp4f*$^{+/+}$ and *Nlrp4f*$^{-/-}$ oocytes were labeled with MitoTracker (red) at GVBD 1-2 h, then fixed and stained with α-tubulin-FITC (green). The astral-like microtubules from spindles were enlarged and are shown on the right. (E) ER and mitochondria were labeled with ER-Tracker (green) and MitoTracker (red) in *Nlrp4f*$^{-/-}$ oocytes treating with DMSO and nocodazole after GVBD (1-2 h). (F) The ovaries of *Nlrp4f*$^{+/+}$ and *Nlrp4f*$^{-/-}$ females were fixed and sectioned for TEM. Representative images of the oocytes from these ovaries were obtained with transmission electron microscopy. White arrows indicate the CPLs. Ace-α-tub, acetylated α-tubulin; α-tub, α-tubulin; Mito, mitochondria. Scale bars: 20 µm (C,D,E); 10 µm (D, enlargement); 500 nm (F).

Development (2019) 146, dev183616. doi:10.1242/dev.183616

The SCMC is required for CPL formation and organelle distribtion

Although the SCMC core protein Nlrp5, Tle6 or Ooep was necessary for the stability of Nlrp4f (Fig. 1F,G), depletion of Nlrp4f did not affect expression levels of SCMC proteins, including Nlrp5, Tle6, Ooep and Zbed3 (Fig. S7A,B). Furthermore, depletion of Nlrp4f did not affect the interactions of these SCMC proteins (Fig. S7C). These results suggest that Nlrp4f is not a core component of the SCMC.

The absence of CPL formation in *Nlrp4f* null oocytes is reminiscent of oocytes depleted of Zbed3, which is also not a core component of the SCMC (Fig. 5F) (Gao et al., 2018). These results suggest that integrity of the SCMC or any of the SCMC proteins is required for the formation of CPLs. To test this, we analyzed CPLs in oocytes depleted of other SCMC proteins. We focused on Tle6, a core SCMC protein, and on Khdc3, another non-core SCMC protein. Our results revealed that the CPLs were largely absent in *Tle6*$^{-/-}$ and *Khdc3*$^{-/-}$ oocytes (Fig. 6A,B). We also observed the aberrant distribution of organelles in *Khdc3*$^{-/-}$ oocytes (Fig. S8). Considering the absence of CPLs and the aberrant distribution of organelles in the oocytes with disrupted Nlrp4f, Khdc3 or Tle6, as well as Zbed3, Nlrp5, Ooep or Padi6 (Fig. 4, Fig. 5F; Fig. S8) (Gao et al., 2018; Kan et al., 2011; Kim et al., 2010; Tashiro et al., 2010; Yurttas et al., 2008), we propose that the SCMC is required for CPL formation and organelle distribution in mouse oocytes.

The SCMC forms before CPL formation during mouse oogenesis

Although CPLs were absent in *Nlrp4f* and *Zbed3* null oocytes, the SCMC was not affected in these oocytes (Fig. 5F; Fig. S7) (Gao et al., 2018), suggesting that the SCMC, or at least its core complex, is the upstream regulator of CPL formation. To test this, we examined the expression of SCMC proteins in normal ovaries at postnatal day (P)1, P2, P3, P5, P10, P17 and P21. Although mRNA levels of the

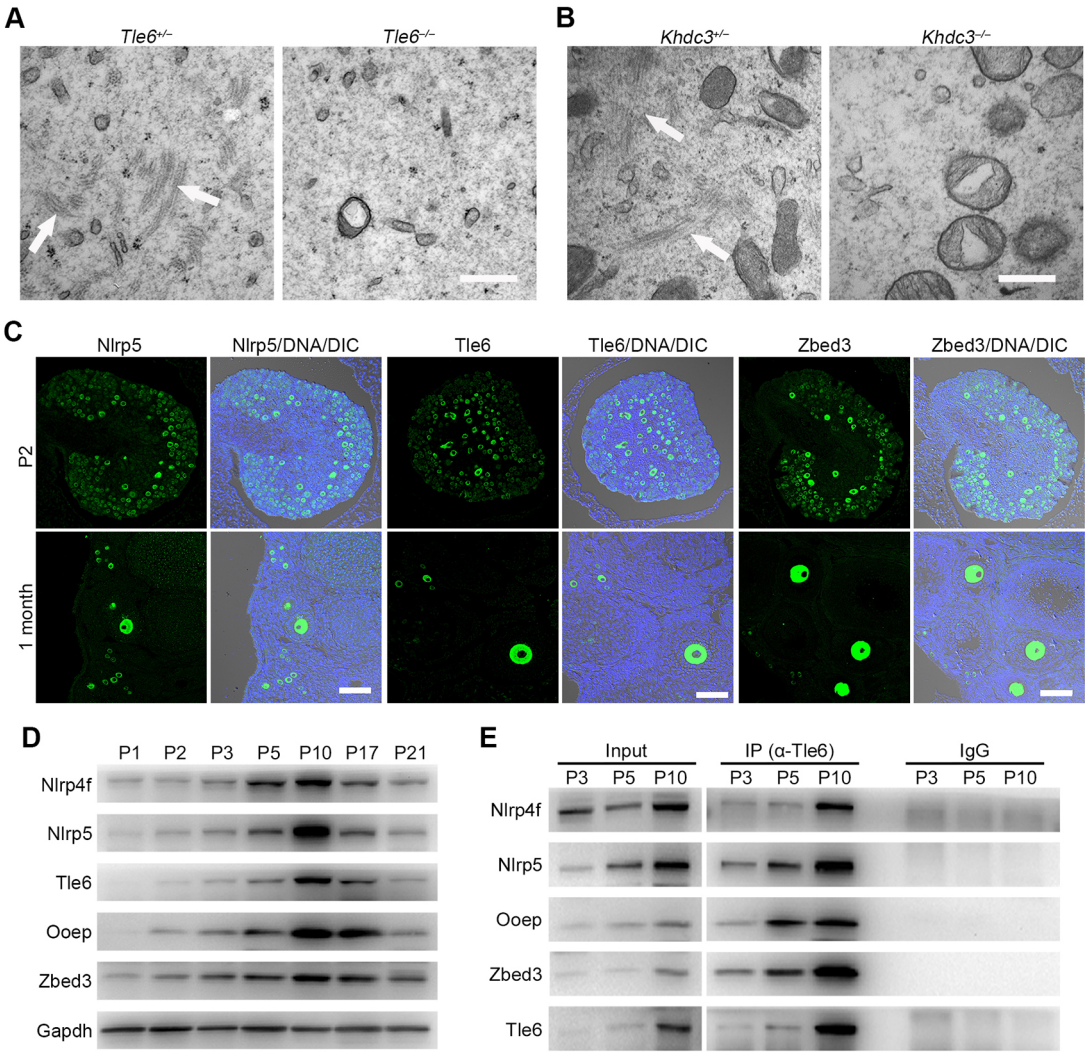

Fig. 6. Formation of CPLs and SCMC in mouse oocytes. (A) TEM images of GV oocytes from *Tle6*$^{+/-}$ and *Tle6*$^{-/-}$ ovaries. White arrows indicate CPLs. (B) TEM images of GV oocytes from *Khdc3*$^{+/-}$ and *Khdc3*$^{-/-}$ ovaries. White arrows indicate CPLs. (C) Paraffin sections of ovaries from postnatal day (P) 2 and one-month-old normal mice were stained with anti-mater, anti-Tle6 and anti-Zbed3 antibodies and Hoechst 33342 (DNA). (D) Ovarian lysates were extracted from normal females of different ages (P1, P2, P3, P5, P10, P17 and P21) and examined by immunoblot with anti-Nlrp4f, anti-Nlrp5, anti-Tle6, anti-Ooep and anti-Zbed3 antibodies, respectively. (E) Normal ovarian lysates of different ages (P3, P5 and P10) were immunoprecipitated with anti-Tle6 antibodies or normal IgG (mouse), followed by immunoblot with specific antibodies. Scale bars: 500 nm (A,B); 100 µm (C).

Development (2019) 146, dev183616. doi:10.1242/dev.183616

SCMC genes *Nlrp4f*, *Ooep*, *Nlrp5*, *Tle6* and *Zbed3* were highly expressed in the ovary when mice were born (Joshi et al., 2007; Li et al., 2008), these SCMC proteins were at low levels in the oocytes of normal mouse ovaries at this stage, as shown by immunostaining and western blotting (Fig. 6C,D). Importantly, these SCMC proteins were specifically co-precipitated by Tle6 antibody in normal ovarian lysates after P3 (Fig. 6E). CPLs were sporadically observed in the oocytes of ovaries at P5-P10, but not observed in oocytes of ovaries at P3 (Wassarman and Josefowicz, 1978; Yurttas et al., 2008; Zamboni, 1970). Thus, our results suggest that the SCMC forms prior to CPLs in the oocytes of mouse ovaries, further supporting the idea that the SCMC is involved in CPL formation.

DISCUSSION

CPLs were first discovered as an abundant structure in mammalian oocytes and early embryos (Gallicano et al., 1991; Hadek, 1966; Weakley, 1966, 1968; Zamboni, 1970). However, the roles and compositions of these structures remain mysterious. Recently, Padi6 was identified as an oocyte- and embryo-specific protein localized in the CPLs of mouse oocytes (Wright et al., 2003). Depletion of *Padi6* resulted in the absence of CPLs and arrested development at the two-cell stage, suggesting that CPLs play a role in development and female fertility (Esposito et al., 2007). More recently, the SCMC core protein Nlrp5 or Ooep was reported to localize to CPLs and be required for CPL formation and two-cell embryo development (Li et al., 2008; Tashiro et al., 2010; Tong et al., 2000). However, disruption of proteins Zbed3, Nlrp4f or Khdc3 also resulted in the loss of CPLs, but the phenotypes were less severe for preimplantation development and female fecundity (Fig. 3, Fig. 5F) (Gao et al., 2018; Zheng and Dean, 2009). These results suggest that disruption of CPL formation is not the major cause of arrested development at the two-cell stage and infertility in *Ooep*, *Nlrp5*, *Tle6* and *Padi6* null females. Consistent with this, a recent report shows that CPL formation may not be related to arrested two-cell development in the mouse (Longo et al., 2018).

CPLs occupy large spaces of cytoplasm in mouse oocytes and early embryos (Capco and McGaughey, 1986; Gallicano et al., 1991; Zamboni, 1970). Some CPLs have been observed to surround the organelles in mouse oocytes (Gao et al., 2018; Kan et al., 2011). These results suggest that CPLs play a role in maintaining the localization of organelles in mouse oocytes. Consistent with this, the absence of CPLs is related to defects in organelle distribution in oocytes with disruption of SCMC proteins Nlrp4f, Zbed3, Khdc3, Nlrp5, Ooep, Tle6 or Padi6 (Fig. 4) (Gao et al., 2018; Kan et al., 2011; Kim et al., 2010; Tashiro et al., 2010; Yurttas et al., 2008). Furthermore, CPLs contain intermediate filaments in mammalian oocytes and early embryos (Capco et al., 1993; Gallicano et al., 1994). The intermediate filaments directly or indirectly interact with other two cytoskeletons comprising microfilaments and microtubules, and regulate the dynamics of cytoskeletons in various cell types (Huber et al., 2015). Thus, CPLs might regulate microfilaments and microtubules in mouse oocytes and early embryos. Consistently, the absence of CPLs is related to the disorganized formation of microfilaments and microtubules in oocytes and embryos with disrupted SCMC genes (Fig. 5) (Gao et al., 2018; Kan et al., 2011; Yu et al., 2014). Thus, CPLs might control organelle redistribution through the cytoskeleton in mouse oocytes and early embryos.

Three SCMC-related proteins, Padi6, Ooep and Nlrp5, are localized to the CPLs of mouse oocytes (Tashiro et al., 2010; Wright et al., 2003). Disruption of all examined SCMC proteins, including Padi6, Nlrp5, Ooep, Tle6, Khdc3, Zbed3 and Nlrp4f, leads to loss of CPLs in mouse oocytes (Fig. 5F, Fig. 6A,B) (Esposito et al., 2007; Gao et al., 2018; Kim et al., 2010; Tashiro et al., 2010). These results suggest that the SCMC is closely related to CPLs or that they are the same structures in mouse oocytes (Kim et al., 2010; Tashiro et al., 2010). However, depletion of Zbed3 and Nlrp4f does not affect the stability of other SCMC proteins (including Nlrp5, Ooep and Tle6) nor the interactions of these proteins (Fig. S7) (Gao et al., 2018), suggesting that the SCMC, or at least the SCMC core complex, is distinct from the CPLs and involved in CPL formation. Consistent with this, SCMC proteins are expressed and interact before CPLs form during mouse oogenesis (Fig. 6C-E) (Wassarman and Josefowicz, 1978). How the SCMC regulates CPL formation remains unknown. One possibility is that all SCMC proteins control CPL formation via a common regulatory factor or pathway. Consistent with this, CPLs are preserved by glutaraldehyde but not by fixatives such as osmium tetroxide, formaldehyde and other short chain aldehydes (Weakley, 1966, 1968).

The molecular mass of the SCMC is larger than the total mass of the first four proteins identified (Ooep, Nlrp5, Tle6 and Khdc3), suggesting additional proteins in this complex (Li et al., 2008, 2013; Lu et al., 2017). Padi6 might also be involved in the SCMC (Kim et al., 2010; Li et al., 2008). Recently, another maternal-effect gene, *Nlrp2*, has been reported to be associated with the SCMC, based on the *in vitro* interactions of Nlrp2 and SCMC proteins, their localization and similar phenotypes (Mahadevan et al., 2017). We have recently characterized Zbed3 as a novel component of the SCMC in mouse oocytes and early embryos (Gao et al., 2018). The SCMC may be conserved in other mammals, including humans (Bebbere et al., 2014; Lu et al., 2017; Zhu et al., 2015). These studies have prompted us to propose that the SCMC is a functional module in the mammalian OET (Lu et al., 2017). Here, we have identified Nlrp4f as a novel protein of the SCMC, further supporting the notion of a functional module of the SCMC. The first NLRP subfamily protein identified in the SCMC was Nlrp5 (Li et al., 2008; Tong et al., 2000). Recently, Nlrp2 was reported to be associated with the SCMC (Kuchmiy et al., 2016; Mahadevan et al., 2017). Similar to the expression patterns of SCMC genes, the transcripts of many NLRP subfamily members, such as Nlrp14, Nlrp4a-4g and Nlrp9a-9c, are specifically expressed in ovarian tissue, oocytes and preimplantation embryos (Hamatani et al., 2004). Thus, some other NLRP proteins might also function in oocytes and early embryos through the SCMC.

In summary, we have characterized Nlrp4f as a novel component of the SCMC in the mouse. The absence of CPLs is related to the disorganized distribution of organelles in oocytes in response to depletion of any SCMC genes, suggesting that the SCMC functions in regulating organelle distribution, probably by the CPLs in mouse oocytes and female fertility. Accumulating evidence suggests that mutations of human SCMC genes are related to female reproductive disorders, including recurrent embryonic loss, molar pregnancies and imprinting disorders (Amoushahi et al., 2019; Begemann et al., 2018; Lu et al., 2017; Mu et al., 2019; Nguyen et al., 2018; Wang et al., 2018). Further studies of phenotypes in Nlrp4f and other SCMC gene mutants and exploration of the relationships between the SCMC and its proteins, CPLs and oocyte quality will contribute to an understanding of human OET and the pathogenesis of reproductive diseases.

MATERIALS AND METHODS

Mice maintenance, oocyte and embryo collection and culture

All animal maintenance and manipulations were performed according to the guidelines of the Animal Care and Use Committee of the Institute of Zoology, Chinese Academy of Sciences.

Development (2019) 146, dev183616. doi:10.1242/dev.183616

Normal and *Nlrp4f*$^{-/-}$ females aged 6-8 weeks were stimulated with 5 IU pregnant mare serum gonadotrophin (PMSG). After 46-48 h, oocytes were recovered by scraping the surface of the ovaries with a 26-gauge needle in M2 medium. MII oocytes were collected at 13-15 h after additional stimulation with 5 IU human chorionic gonadotrophin (hCG). Zygotes, two-cell embryos, morulae and blastocysts from normal and *Nlrp4f*$^{-/-}$ mice were collected at 24, 48, 72 and 96 h after hCG stimulation, respectively.

For *in vitro* culture, two-cell embryos were collected from *Nlrp4f*$^{+/+}$ and *Nlrp4f*$^{-/-}$ females mated with normal fertile males. These two-cell embryos were cultured in KSOM medium (Millipore, MR-121-D) at 37°C in 5% CO_2. The development of embryos was examined every 4 h and the developmental rates of the embryos were calculated.

Oocyte extraction and mass spectrometry

Equal numbers of oocytes (~500 GV oocytes) were collected from *Nlrp5*$^{+/+}$, *Nlrp5*$^{+/-}$ and *Nlrp5*$^{-/-}$ mice and extracted with buffer containing 100 mM NaCl, 3 mM $MgCl_2$, 300 mM sucrose, 10 mM PIPES (pH 6.8), 0.5% Triton X-100 and 1× Complete Protease Inhibitor Cocktail (Roche) for 30 min at room temperature. After extraction, the oocytes were manually picked up as the insoluble fraction. The remains contained the soluble components of oocytes in the buffer. These samples were separated by SDS-PAGE and stained with Coomassie Brilliant Blue (SimplyBlu SafeStain, Invitrogen, LC6060) according to the manufacturer's protocol. The specific bands in *Nlrp5*$^{+/+}$ (wild type) and *Nlrp5*$^{+/-}$, but not *Nlrp5*$^{-/-}$, oocytes were collected for mass spectrometry (NanoLC-LTQ-Orbitrap XL, Thermo Finnigan).

Generation of *Nlrp4f* knockout mice using CRISPR/Cas9

As previously reported, the T7 promoter was added to the Cas9 encoding region using pX330 as the template (Yang et al., 2013). Cas9 PCR products were transcribed *in vitro* using *mMESSAGE* mMACHINE T7 ULTRA Kit (Ambion, AM1345). The *Nlrp4f* single guide RNAs (sgRNAs) were designed using the online CRISPR design tool (http://crispr.mit.edu/) and cloned into the pUC57-sgRNA expression vector. The sgRNA PCR templates were amplified for *in vitro* transcription with *MAXIscript* SP6/T7 In Vitro Transcription Kit, according to the manufacturer's protocol (Ambion, AM1322). Then, 50 ng/µl of *Cas9* mRNA and 25 ng/µl of sgRNAs were mixed and injected into the cytoplasm of CD1 mouse zygotes. The surviving zygotes were transplanted into the oviducts of pseudopregnant females to produce the offspring. The offspring were genotyped by PCR with specific primers for *Nlrp4f*: forward primer, 5′-CTGAGGTCCCAGCTTGTGTC-3′; reverse primer, 5′-TTGGCCCTATGGTAGATGCG-3′.

Fertility assessment

For assessing the fertility of male mice, two-month-old *Nlrp4f*$^{+/+}$ females were mated with *Nlrp4f*$^{+/+}$ and *Nlrp4f*$^{-/-}$ male mice by 2:1 co-caging. To test the fertility of female mice, two-month-old *Nlrp4f*$^{+/+}$ and *Nlrp4f*$^{-/-}$ female mice were mated with normal fertile males by 2:1 co-caging. The number of pups per litter was recorded. The results were calculated after they had mated for three consecutive months.

Antibodies

Rabbit anti-Nlrp4f antibody was generated with a standard protocol from Abmart (Shanghai, China). In brief, two peptides selected from Nlrp4f were expressed in *Escherichia coli* Rosetta and purified with Ni^{2+} affinity columns. The purified peptides were mixed and used to immunize rabbits four times. The serum (antibody) from the immunized rabbits was purified with Protein A. The sequence of Nlrp4f peptide 1 was: LSNCSLSEQCWDYLSEVLRQNKTLSHLDISSNDLKDEGLKILCRSLI LPYCVLESLCLSCCGITERGCQDLAEVLKNNQNLKYLHVSYNKLK DTGVMLLCDAIKHPNCHLKDLQLEACEITDASNEELCYAFMQCET LQTLNLMGNAFEV and that of Nlrp4f peptide 2 was: SKNIHHKLYQ CLETLSGNAELQEQIDGMRLFSCLFEMEDEAFLVKAMNCMQQINF VAKNYSDFIVAAYCLKHCSTLKKLSFSTENVLNEGDQSYMEELLIC WNNMCSVFVRSKDIQELRIKDTNFNEPAIRVLYESLKYPSFTLNKL VAN. Primary and secondary antibodies were used as in Table S1.

H&E and immunofluorescent staining

The ovaries from two-month-old females at different ages were fixed in Bouin solution overnight at room temperature for H&E staining or fixed with 4% paraformaldehyde (PFA) in PBS overnight at 4°C for immunofluorescence staining, then embedded in paraffin and sectioned. The sections were dewaxed, rehydrated and stained with H&E. For immunostaining, the rehydrated sections were treated for antigen retrieval and washed three times with PBS. The sections were blocked with 5% BSA for 1 h at room temperature and incubated with primary antibodies (Table S1) overnight at 4°C. After washing three times with PBS, the sections were incubated with secondary antibodies (Table S1) and Hochest 33342 for 1 h at room temperature and then mounted for imaging.

For whole-mount staining of oocytes and early embryos, the isolated oocytes and embryos were fixed with 4% PFA containing 0.5% Triton X-100 for 30 min at room temperature. The immunostaining was performed with primary and secondary antibodies as described above.

For classification of NSN-type and SN-type fully grown oocytes, the oocytes were fixed with 4% PFA, permeabilized with 0.5% Triton X-100, blocked with 5% normal donkey serum and the DNA stained with Hochest 33342. According to their chromatin configuration in the nucleus, oocytes were classified into three groups: nonsurrounded nucleolus (NSN) type with diffused chromatin, surrounded nucleolus (SN) type with a typical ring chromatin and middle type with diffused and half-ring chromatin. The images were acquired with a LSM780 (Zeiss).

Immunoblot and co-immunoprecipitation

For immunoblot, different tissues were collected from CD1 mice. Total proteins were extracted using RIPA lysis buffer containing 50 mM Tris-HCl (pH 7.5), 150 mM NaCl, 1% sodium deoxycholate, 1% Triton X-100, 0.1% SDS, 5 mM EDTA, 1 mM Na_3VO_4, 5-10 mM NaF and complete EDTA-free Protease Inhibitor Cocktail (Roche). The lysate was incubated on ice for 15 min and centrifuged at 12,000 rpm (13,800 ***g***) for 15 min at 4°C. The supernatant was quantified using a BCA reagent kit (Beyotime, P0012-1). For oocyte samples, equal numbers of oocytes (50-200) were collected. Then, proteins were separated by 8-15% SDS-PAGE and transferred onto a PVDF membrane. The membrane was pretreated with 5% defatted milk for 1 h at room temperature and incubated with primary antibodies (Table S1) overnight at 4°C. After washing three times with PBS containing Tween-20, the membrane was incubated with horseradish peroxidase (HRP)-conjugated secondary antibodies (Table S1) for 1 h at room temperature. Signals were developed with SuperSignal West Pico Chemiluminescent Substrate (Thermo Fisher Scientific, 34080) and analyzed with Quantity One software (Bio-Rad Laboratories).

For co-immunoprecipitation, ovaries were isolated from CD1 female mice of different ages. Total proteins were extracted using immunoprecipitation (IP) lysis buffer containing 25 mM Tris-HCl (pH 7.5), 150 mM NaCl, 1 mM EDTA, 1% NP-40, 5% glycerol, 1 mM Na_3VO_4, 2 mM NaF and complete EDTA-free Protease Inhibitor Cocktail (Roche). BSA (final concentration 1%) was also added to samples of GV oocytes to protect proteins from degradation. After centrifugation [12,000 rpm (13,800 ***g***) for 15 min at 4°C], the lysates were incubated with mouse anti-Tle6 antibody or normal mouse IgG at 4°C for 3-4 h before Protein A/G magnetic beads (Selleck, B23202) were added. After an additional incubation for 3 h at 4°C, beads were washed five times with IP lysis buffer and eluted with 1× SDS loading buffer. The samples were separated by SDS-PAGE, and western blot performed using specific antibodies.

Quantitative real-time PCR

According to the manufacturer's protocols, mRNAs of different tissues were extracted using RNAzol reagent (Molecular Research Center, RN190) and mRNA of mouse eggs or embryos was isolated using Dynabeads mRNA DIRECT Micro Kit (Life Technologies, 61021). Complementary DNA (cDNA) was synthesized using PrimeScript RT Reagent Kit (Takara, RR037A). Quantitative RT-PCR was conducted with EvaGreen 2× qPCR MasterMix (Applied Biological Materials, MasterMix-S). The expression of target genes was normalized with *Gapdh*. *Nlrp4f* forward primer, 5′-TCATCCAACACTTGCTCCAGC-3′; *Nlrp4f* reverse primer, 5′-AAA-GATGCCATCTTGTCTTCAGG-3′; *Gapdh* forward

primer, 5'-CCCCAATGTGTCCGTCGTG-3'; and *Gapdh* reverse primer, 5'-TGCCTGCTTCACCACCTTCT-3'.

Mitochondria and ER labeling

Before live-imaging, mouse oocytes and zygotes were cultured in M2 and KSOM medium, respectively, with MitoTracker Red CMXRos (1:10,000; Invitrogen, M7512) and ER-Tracker Blue-White DPX (1:5000; Invitrogen, E12353) at 37°C in 5% CO_2 for 60 min. The pictures of live imaging were captured by UltraVIEW-VoX (Perkin Elmer).

For drug treatment, *Nlrp4f*$^{+/+}$ and *Nlrp4f*$^{-/-}$ GV oocytes were cultured in M2 medium supplemented with 3-isobutyl-1-methylxanthine (IBMX, 100 µg/ ml; Sigma-Aldrich, I7018) and with DMSO, TSA (2 µg/ ml for 12 h; Beyotime, S1893) or nocodazole (2.5 µg/ ml for 2 h at 37°C in 5% CO_2; Sigma-Aldrich, M1404). These arrested oocytes were washed three times with M2 medium to release IBMX inhibition, cultured to GVBD in M2 medium with DMSO, TSA or nocodazole, and labeled with MitoTracker Red CMXRos.

Transmission electron microscopy

TEM was performed as previously described (Gao et al., 2018). Briefly, the ovaries were isolated from two-month-old females and fixed in buffer containing 2.5% glutaraldehyde, 4% PFA and 0.1 M Na-cacodylate for 24 h at 4°C. After gradient dehydration, the samples were embedded in LX112 resin and cut into ultrathin sections. Oocytes from the ovarian sections were imaged using TEM (Jeol, JEM-1230).

Statistical analysis

All experiments were performed at least three times with different samples. All statistics were analyzed by the Student's *t*-test in GraphPad Prism5 software and presented as mean±s.e.m. **P*<0.05 was considered significant.

Acknowledgements

We thank Lijuan Wang, Shiwen Li, Xili Zhu and Hua Qin (Institute of Zoology Chinese Academy of Science) for technical assistance, and Dr Jurrien Dean at the National Institutes of Health in the USA, Dr Marcel van Duin at the Ferring Pharmaceuticals and Dr Nicolas Plachta at Agency for Science, Technology and Research (Singapore) for their critical review of the manuscript.

Competing interests

The authors declare no competing or financial interests.

Author contributions

Conceptualization: D.Q., Z.G., L.L.; Methodology: D.Q., X.Y.; Validation: D.Q., Z.G., Y.X., X.N.; Formal analysis: D.Q., Z.G., Q.-Y.S., Z.Y., L.L.; Investigation: D.Q., Z.G., Y.X., X.Z., H.M., X.Y., X.N., N.F., X.W., Y.O.; Resources: Y.X., Y.O., Q.-Y.S., Z.Y., L.L.; Data curation: D.Q., Z.G., H.M., N.F., Z.Y.; Writing - original draft: D.Q.; Writing - review & editing: Z.Y., L.L.; Visualization: L.L.; Supervision: L.L.; Project administration: X.Z., L.L.; Funding acquisition: L.L.

Funding

The work was supported by the National Key R&D Program of China (2018YFC1004500), the National Natural Science Foundation of China (31930033, 31590832 and 31771633) and the Strategic Collaborative Research Program of the Ferring Institute of Reproductive Medicine, Ferring Pharmaceuticals and Chinese Academy of Sciences (FIRMB180202).

Supplementary information

Supplementary information available online at
http://dev.biologists.org/lookup/doi/10.1242/dev.183616.supplemental

References

Alazami, A. M., Awad, S. M., Coskun, S., Al-Hassan, S., Hijazi, H., Abdulwahab, F. M., Poizat, C. and Alkuraya, F. S. (2015). TLE6 mutation causes the earliest known human embryonic lethality. *Genome Biol.* **16**, 240. doi:10.1186/s13059-015-0792-0

Amoushahi, M., Sunde, L. and Lykke-Hartmann, K. (2019). The pivotal roles of the NOD-like receptors with a PYD domain, NLRPs, in oocytes and early embryo development. *Biol. Reprod.* **101**, 284-296. doi:10.1093/biolre/ioz098

Bebbere, D., Ariu, F., Bogliolo, L., Masala, L., Murrone, O., Fattorini, M., Falchi, L. and Ledda, S. (2014). Expression of maternally derived KHDC3, NLRP5, OOEP and TLE6 is associated with oocyte developmental competence in the ovine species. *BMC Dev. Biol.* **14**, 40. doi:10.1186/s12861-014-0040-y

Begemann, M., Rezwan, F. I., Beygo, J., Docherty, L. E., Kolarova, J., Schroeder, C., Buiting, K., Chokkalingam, K., Degenhardt, F., Wakeling, E. L. et al. (2018). Maternal variants in NLRP and other maternal effect proteins are associated with multilocus imprinting disturbance in offspring. *J. Med. Genet.* **55**, 497-504. doi:10.1136/jmedgenet-2017-105190

Capco, D. G. and McGaughey, R. W. (1986). Cytoskeletal reorganization during early mammalian development: analysis using embedment-free sections. *Dev. Biol.* **115**, 446-458. doi:10.1016/0012-1606(86)90265-4

Capco, D. G., Gallicano, G. I., McGaughey, R. W., Downing, K. H. and Larabell, C. A. (1993). Cytoskeletal sheets of mammalian eggs and embryos: a lattice-like network of intermediate filaments. *Cell Motil. Cytoskeleton* **24**, 85-99. doi:10.1002/cm.970240202

Christians, E., Davis, A. A., Thomas, S. D. and Benjamin, I. J. (2000). Maternal effect of Hsf1 on reproductive success. *Nature* **407**, 693-694. doi:10.1038/35037669

Condic, M. L. (2016). The role of maternal-effect genes in mammalian development: are mammalian embryos really an exception? *Stem Cell Rev. Rep.* **12**, 276-284. doi:10.1007/s12015-016-9648-6

Dadé, S., Callebaut, I., Paillisson, A., Bontoux, M., Dalbiès-Tran, R. and Monget, P. (2004). In silico identification and structural features of six new genes similar to MATER specifically expressed in the oocyte. *Biochem. Biophys. Res. Commun.* **324**, 547-553. doi:10.1016/j.bbrc.2004.09.086

Docherty, L. E., Rezwan, F. I., Poole, R. L., Turner, C. L. S., Kivuva, E., Maher, E. R., Smithson, S. F., Hamilton-Shield, J. P., Patalan, M., Gizewska, M. et al. (2015). Mutations in NLRP5 are associated with reproductive wastage and multilocus imprinting disorders in humans. *Nat. Commun.* **6**, 8086. doi:10.1038/ncomms9086

Esposito, G., Vitale, A. M., Leijten, F. P. J., Strik, A. M., Koonen-Reemst, A. M. C. B., Yurttas, P., Robben, T. J. A. A., Coonrod, S. and Gossen, J. A. (2007). Peptidylarginine deiminase (PAD) 6 is essential for oocyte cytoskeletal sheet formation and female fertility. *Mol. Cell Endocrinol.* **273**, 25-31. doi:10.1016/j.mce.2007.05.005

Fernandes, R., Tsuda, C., Perumalsamy, A. L., Naranian, T., Chong, J., Acton, B. M., Tong, Z.-B., Nelson, L. M. and Jurisicova, A. (2012). NLRP5 mediates mitochondrial function in mouse oocytes and embryos. *Biol. Reprod.* **86**, 138, 1-10. doi:10.1095/biolreprod.111.093583

Gallicano, G. I., McGaughey, R. W. and Capco, D. G. (1991). Cytoskeleton of the mouse egg and embryo: reorganization of planar elements. *Cell Motil. Cytoskeleton* **18**, 143-154. doi:10.1002/cm.970180209

Gallicano, G. I., Larabell, C. A., McGaughey, R. W. and Capco, D. G. (1994). Novel cytoskeletal elements in mammalian eggs are composed of a unique arrangement of intermediate filaments. *Mech. Dev.* **45**, 211-226. doi:10.1016/0925-4773(94)90009-4

Gao, Z., Zhang, X., Yu, X., Qin, D., Xiao, Y., Yu, Y., Xiang, Y., Nie, X., Lu, X., Liu, W. et al. (2018). Zbed3 participates in the subcortical maternal complex and regulates the distribution of organelles. *J. Mol. Cell Biol.* **10**, 74-88. doi:10.1093/jmcb/mjx035

Hadek, R. (1966). Cytoplasmic whorls in the golden hamster oocyte. *J. Cell Sci.* **1**, 281-282.

Hamatani, T., Falco, G., Carter, M. G., Akutsu, H., Stagg, C. A., Sharov, A. A., Dudekula, D. B., VanBuren, V. and Ko, M. S. (2004). Age-associated alteration of gene expression patterns in mouse oocytes. *Hum. Mol. Genet.* **13**, 2263-2278. doi:10.1093/hmg/ddh241

Huber, F., Boire, A., López, M. P. and Koenderink, G. H. (2015). Cytoskeletal crosstalk: when three different personalities team up. *Curr. Opin. Cell Biol.* **32**, 39-47. doi:10.1016/j.ceb.2014.10.005

Joshi, S., Davies, H., Sims, L. P., Levy, S. E. and Dean, J. (2007). Ovarian gene expression in the absence of FIGLA, an oocyte-specific transcription factor. *BMC Dev. Biol.* **7**, 67. doi:10.1186/1471-213X-7-67

Kan, R., Yurttas, P., Kim, B., Jin, M., Wo, L., Lee, B., Gosden, R. and Coonrod, S. A. (2011). Regulation of mouse oocyte microtubule and organelle dynamics by PADI6 and the cytoplasmic lattices. *Dev. Biol.* **350**, 311-322. doi:10.1016/j.ydbio.2010.11.033

Kim, B., Kan, R., Anguish, L., Nelson, L. M. and Coonrod, S. A. (2010). Potential role for MATER in cytoplasmic lattice formation in murine oocytes. *PLoS ONE* **5**, e12587. doi:10.1371/journal.pone.0012587

Kuchmiy, A. A., D'Hont, J., Hochepied, T. and Lamkanfi, M. (2016). NLRP2 controls age-associated maternal fertility. *J. Exp. Med.* **213**, 2851-2860. doi:10.1084/jem.20160900

Li, L., Baibakov, B. and Dean, J. (2008). A subcortical maternal complex essential for preimplantation mouse embryogenesis. *Dev. Cell* **15**, 416-425. doi:10.1016/j.devcel.2008.07.010

Li, L., Zheng, P. and Dean, J. (2010). Maternal control of early mouse development. *Development* **137**, 859-870. doi:10.1242/dev.039487

Li, L., Lu, X. and Dean, J. (2013). The maternal to zygotic transition in mammals. *Mol. Aspects Med.* **34**, 919-938. doi:10.1016/j.mam.2013.01.003

Longo, M., Boiani, M., Redi, C. A. and Monti, M. (2018). Cytoplasmic lattices are not linked to mouse 2-cell embryos developmental arrest. *Eur. J. Histochem.* **62**. doi:10.4081/ejh.2018.2972

Lu, X., Gao, Z., Qin, D. and Li, L. (2017). A maternal functional module in the mammalian oocyte-to-embryo transition. *Trends Mol. Med.* **23**, 1014-1023. doi:10.1016/j.molmed.2017.09.004

Mahadevan, S., Sathappan, V., Utama, B., Lorenzo, I., Kaskar, K. and Van den Veyver, I. B. (2017). Maternally expressed NLRP2 links the subcortical maternal complex (SCMC) to fertility, embryogenesis and epigenetic reprogramming. *Sci. Rep.* **7**, 44667. doi:10.1038/srep44667

Martinon, F., Gaide, O., Pétrilli, V., Mayor, A. and Tschopp, J. (2007). NALP inflammasomes: a central role in innate immunity. *Semin. Immunopathol.* **29**, 213-229. doi:10.1007/s00281-007-0079-y

Monk, D., Sanchez-Delgado, M. and Fisher, R. (2017). NLRPs, the subcortical maternal complex and genomic imprinting. *Reproduction* **154**, R161-R170. doi:10.1530/REP-17-0465

Mu, J., Wang, W., Chen, B., Wu, L., Li, B., Mao, X., Zhang, Z., Fu, J., Kuang, Y., Sun, X. et al. (2019). Mutations in NLRP2 and NLRP5 cause female infertility characterised by early embryonic arrest. *J. Med. Genet.* **56**, 471-480. doi:10.1136/jmedgenet-2018-105936

Murdoch, S., Djuric, U., Mazhar, B., Seoud, M., Khan, R., Kuick, R., Bagga, R., Kircheisen, R., Ao, A., Ratti, B. et al. (2006). Mutations in NALP7 cause recurrent hydatidiform moles and reproductive wastage in humans. *Nat. Genet.* **38**, 300-302. doi:10.1038/ng1740

Nguyen, N. M. P., Khawajkie, Y., Mechtouf, N., Rezaei, M., Breguet, M., Kurvinen, E., Jagadeesh, S., Solmaz, A. E., Aguinaga, M., Hemida, R. et al. (2018). The genetics of recurrent hydatidiform moles: new insights and lessons from a comprehensive analysis of 113 patients. *Mod. Pathol.* **31**, 1116-1130. doi:10.1038/s41379-018-0031-9

Parry, D. A., Logan, C. V., Hayward, B. E., Shires, M., Landolsi, H., Diggle, C., Carr, I., Rittore, C., Touitou, I., Philibert, L. et al. (2011). Mutations causing familial biparental hydatidiform mole implicate C6orf221 as a possible regulator of genomic imprinting in the human oocyte. *Am. J. Hum. Genet.* **89**, 451-458. doi:10.1016/j.ajhg.2011.08.002

Ratsimandresey, R. A., Dorfleutner, A. and Stehlik, C. (2013). An update on PYRIN domain-containing pattern recognition receptors: from immunity to pathology. *Front. Immunol.* **4**, 440. doi:10.3389/fimmu.2013.00440

Rezaei, M., Nguyen, N. M. P., Foroughinia, L., Dash, P., Ahmadpour, F., Verma, I. C., Slim, R. and Fardaei, M. (2016). Two novel mutations in the KHDC3L gene in Asian patients with recurrent hydatidiform mole. *Hum. Genome Var.* **3**, 16027. doi:10.1038/hgv.2016.27

Tashiro, F., Kanai-Azuma, M., Miyazaki, S., Kato, M., Tanaka, T., Toyoda, S., Yamato, E., Kawakami, H., Miyazaki, T. and Miyazaki, J.-I. (2010). Maternal-effect gene Ces5/Ooep/Moep19/Floped is essential for oocyte cytoplasmic lattice formation and embryonic development at the maternal-zygotic stage transition. *Genes Cells* **15**, 813-828. doi:10.1111/j.1365-2443.2010.01420.x

Tong, Z.-B., Gold, L., Pfeifer, K. E., Dorward, H., Lee, E., Bondy, C. A., Dean, J. and Nelson, L. M. (2000). Mater, a maternal effect gene required for early embryonic development in mice. *Nat. Genet.* **26**, 267-268. doi:10.1038/81547

Wang, X., Song, D., Mykytenko, D., Kuang, Y., Lv, Q., Li, B., Chen, B., Mao, X., Xu, Y., Zukin, V. et al. (2018). Novel mutations in genes encoding subcortical maternal complex proteins may cause human embryonic developmental arrest. *Reprod. Biomed. Online* **36**, 698-704. doi:10.1016/j.rbmo.2018.03.009

Wassarman, P. M. and Josefowicz, W. J. (1978). Oocyte development in the mouse: an ultrastructural comparison of oocytes isolated at various stages of growth and meiotic competence. *J. Morphol.* **156**, 209-235. doi:10.1002/jmor.1051560206

Weakley, B. S. (1966). Electron microscopy of the oocyte and granulosa cells in the developing ovarian follicles of the golden hamster (Mesocricetus auratus). *J. Anat.* **100**, 503-534.

Weakley, B. S. (1968). Comparison of cytoplasmic lamellae and membranous elements in the oocytes of five mammalian species. *Z. Zellforsch. Mikrosk. Anat.* **85**, 109-123. doi:10.1007/BF00330591

Wright, P. W., Bolling, L. C., Calvert, M. E., Sarmento, O. F., Berkeley, E. V., Shea, M. C., Hao, Z., Jayes, F. C., Bush, L. A., Shetty, J. et al. (2003). ePAD, an oocyte and early embryo-abundant peptidylarginine deiminase-like protein that localizes to egg cytoplasmic sheets. *Dev. Biol.* **256**, 74-89. doi:10.1016/S0012-1606(02)00126-4

Yang, H., Wang, H., Shivalila, C. S., Cheng, A. W., Shi, L. and Jaenisch, R. (2013). One-step generation of mice carrying reporter and conditional alleles by CRISPR/Cas-mediated genome engineering. *Cell* **154**, 1370-1379. doi:10.1016/j.cell.2013.08.022

Yu, X.-J., Yi, Z., Gao, Z., Qin, D., Zhai, Y., Chen, X., Ou-Yang, Y., Wang, Z.-B., Zheng, P., Zhu, M.-S. et al. (2014). The subcortical maternal complex controls symmetric division of mouse zygotes by regulating F-actin dynamics. *Nat. Commun.* **5**, 4887. doi:10.1038/ncomms5887

Yurttas, P., Vitale, A. M., Fitzhenry, R. J., Cohen-Gould, L., Wu, W., Gossen, J. A. and Coonrod, S. A. (2008). Role for PADI6 and the cytoplasmic lattices in ribosomal storage in oocytes and translational control in the early mouse embryo. *Development* **135**, 2627-2636. doi:10.1242/dev.016329

Zambetti, L. P., Laudisi, F., Licandro, G., Ricciardi-Castagnoli, P. and Mortellaro, A. (2012). The rhapsody of NLRPs: master players of inflammation … and a lot more. *Immunol. Res.* **53**, 78-90. doi:10.1007/s12026-012-8272-z

Zamboni, L. (1970). Ultrastructure of mammalian oocytes and ova. *Biol. Reprod.* **2** Suppl. 2, 44-63. doi:10.1095/biolreprod2.Supplement_2.44

Zheng, P. and Dean, J. (2009). Role of Filia, a maternal effect gene, in maintaining euploidy during cleavage-stage mouse embryogenesis. *Proc. Natl. Acad. Sci. USA* **106**, 7473-7478. doi:10.1073/pnas.0900519106

Zhu, K., Yan, L., Zhang, X., Lu, X., Wang, T., Yan, J., Liu, X., Qiao, J. and Li, L. (2015). Identification of a human subcortical maternal complex. *Mol. Hum. Reprod.* **21**, 320-329. doi:10.1093/molehr/gau116

Figure S1

A

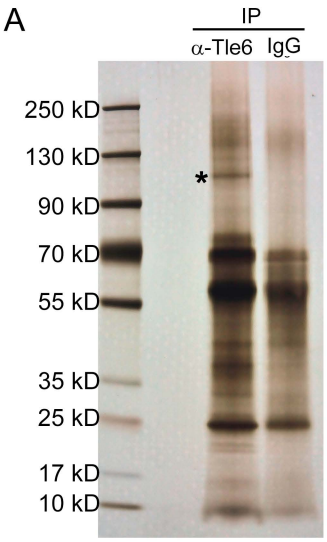

B

Proteins	Score	Coverage	Peptides	MV(kDa)
Nlrp5	80.69	39.06	36	125.4
Tle6	51.80	44.92	20	65.0
Ooep	5.44	25.00	4	18.4
Khdc3	22.77	42.49	12	37.9
Zbed3	11.76	34.21	9	25.6
Nlrp4f	22.54	18.89	14	107.8

Figure S1. Identification of Nlrp4f as a potential component of the SCMC by mass spectrometry (Modified from our previous report (Gao et al., 2018)). (A) Normal GV oocytes were precipitated with anti-Tle6 antibody, and IgG (negative control). The precipitated produces were separated by SDS-PAGE, examined by silver staining and analyzed by mass spectrometry. The asterisk indicated the possible band of Nlrp4f estimated by its molecular weight. (B) The information of mass spectrometry was shown for the known SCMC components and Nlrp4f.

Figure S2

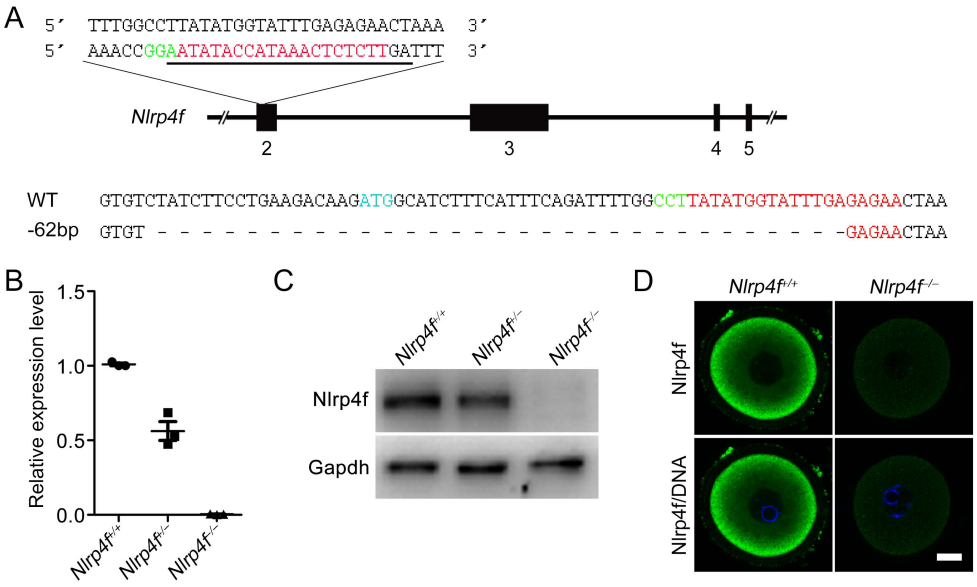

Figure S2. Generation of *Nlrp4f* knockout mice. (A) A schematic of the generation of *Nlrp4f* knockout mice using CRISPR/Cas9. The black rectangles are exons. The sgRNA-targeting sequence is underlined and shown in red, and the protospacer-adjacent motif (PAM) sequence is in green. The initiation codon ATG was labeled in blue. The sequences of normal (WT) and mutant alleles of the founder mice were also shown. (B) qRT-PCR analysis of *Nlrp4f* mRNA expression in *Nlrp4f*$^{+/+}$, *Nlrp4f*$^{-/+}$ and *Nlrp4f*$^{-/-}$ oocytes. The data was normalized to the abundance of *Gapdh* mRNA. The results were from three independent experiments. (C) Immunoblot analysis of Nlrp4f expression in *Nlrp4f*$^{+/+}$, *Nlrp4f*$^{-/+}$ and *Nlrp4f*$^{-/-}$ MII oocytes. Gapdh was used as an internal reference. (D) Immunofluorescent staining of GV oocytes from *Nlrp4f*$^{+/+}$ and *Nlrp4f*$^{-/-}$ mice with Nlrp4f antibody and Hochest 33342 (DNA). Scale bar: 20 μm.

Figure S3

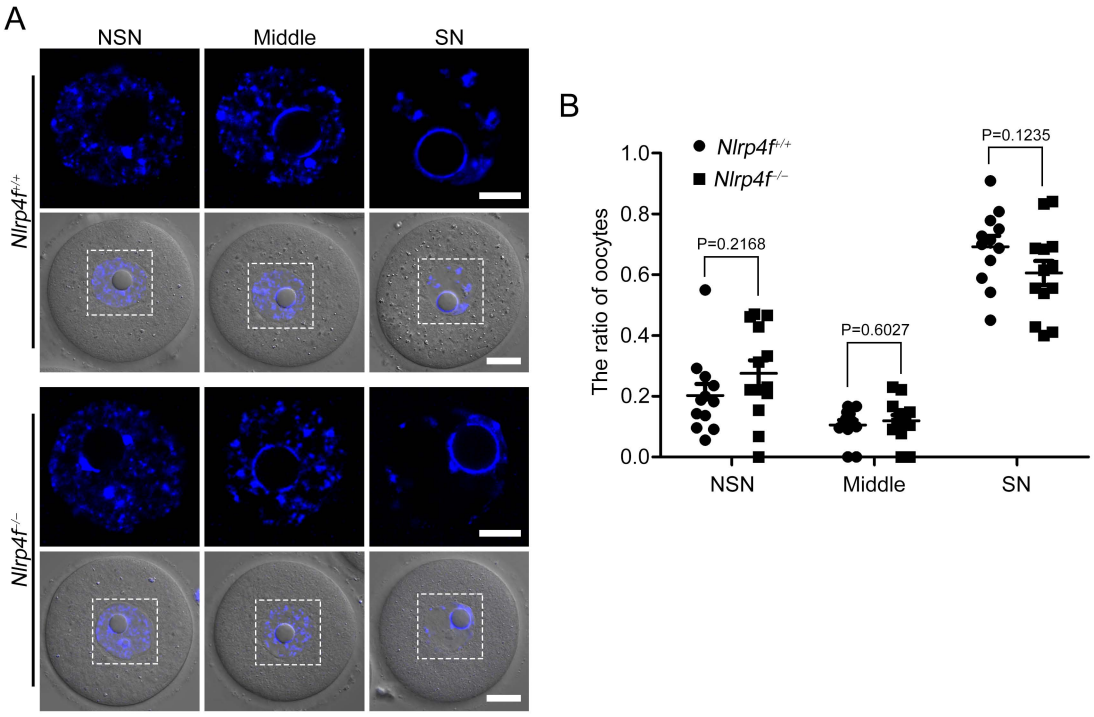

Figure S3. Chromatin configurations in fully grown oocytes. (A) Fully grown oocytes from *Nlrp4f*$^{+/+}$ and *Nlrp4f*$^{-/-}$ females were stained with Hochest 33342 for DNA. According to their chromatin configuration of DNA, the oocytes were classified into three types, NSN, Middle and SN type. The nucleus was dotted with white color and magnified. Scale bar in the upper panel: 10 μm. Scale bar in the down panel: 20 μm. (B) GV oocytes from *Nlrp4f*$^{+/+}$ (n = 12) and *Nlrp4f*$^{-/-}$ (n = 13) female mice were classified into three groups, and the ratio was calculated by the number of NSN, Middle and SN dividing the number of total oocytes. Error bars, s.e.m.

Figure S4

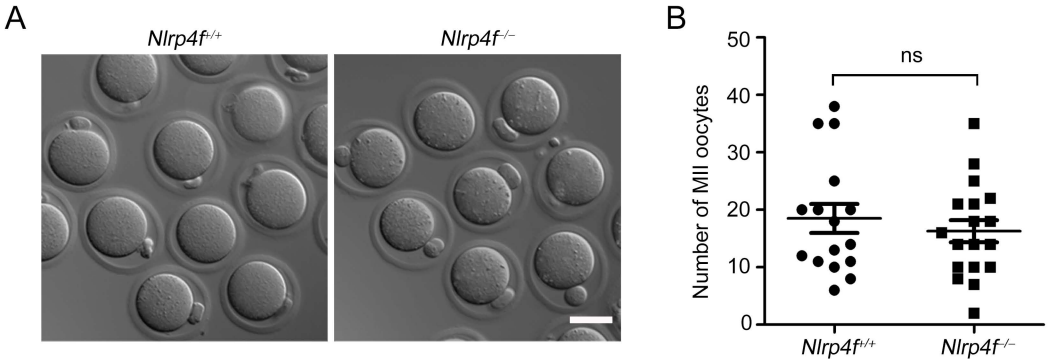

Figure S4. Ovulation in *Nlrp4f* null mice. (A) Representative images of bright field of *Nlrp4f*$^{+/+}$ and *Nlrp4f*$^{-/-}$ MII oocytes after superovulation. Scale bar: 50 μm. (B) The number of MII oocytes from *Nlrp4f*$^{+/+}$ and *Nlrp4f*$^{-/-}$ mice after superovulation. Error bars, s.e.m. ns, no significant.

Figure S5

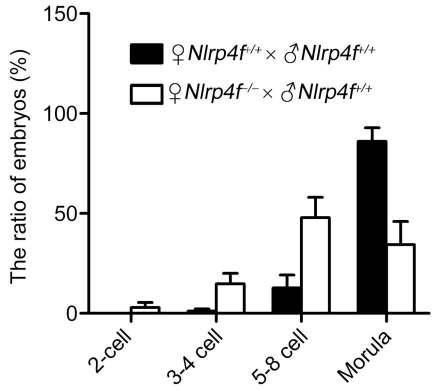

Figure S5. Abnormal development in embryos with depletion of maternal Nlrp4f. The ratio of embryos at different development stages from *Nlrp4f*$^{+/+}$ and *Nlrp4f*$^{-/-}$ females at E2.5.

Figure S6

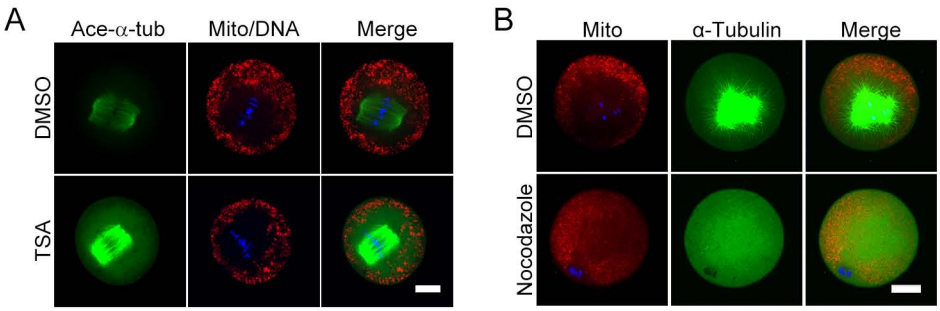

Figure S6. Drug treatment of *Nlrp4f*$^{-/-}$ oocytes. (A) *Nlrp4f*$^{-/-}$ oocytes were labeled with MitoTracker (red) after the treatment with DMSO or TSA at GVBD 1-2 h, then fixed and stained with anti-acetylated-α-tubulin antibody (Ace-α-tubulin, green) and Hochest 33342 (DNA, blue). Scale bar: 20 μm. (B) *Nlrp4f*$^{-/-}$ oocytes were labeled with MitoTracker (red) the treatment with DMSO or Nocodazole at GVBD 1-2 h, then fixed and stained with anti-α-tubulin antibody (green) and Hochest33342 (DNA, blue). Scale bar: 20 μm.

Figure S7

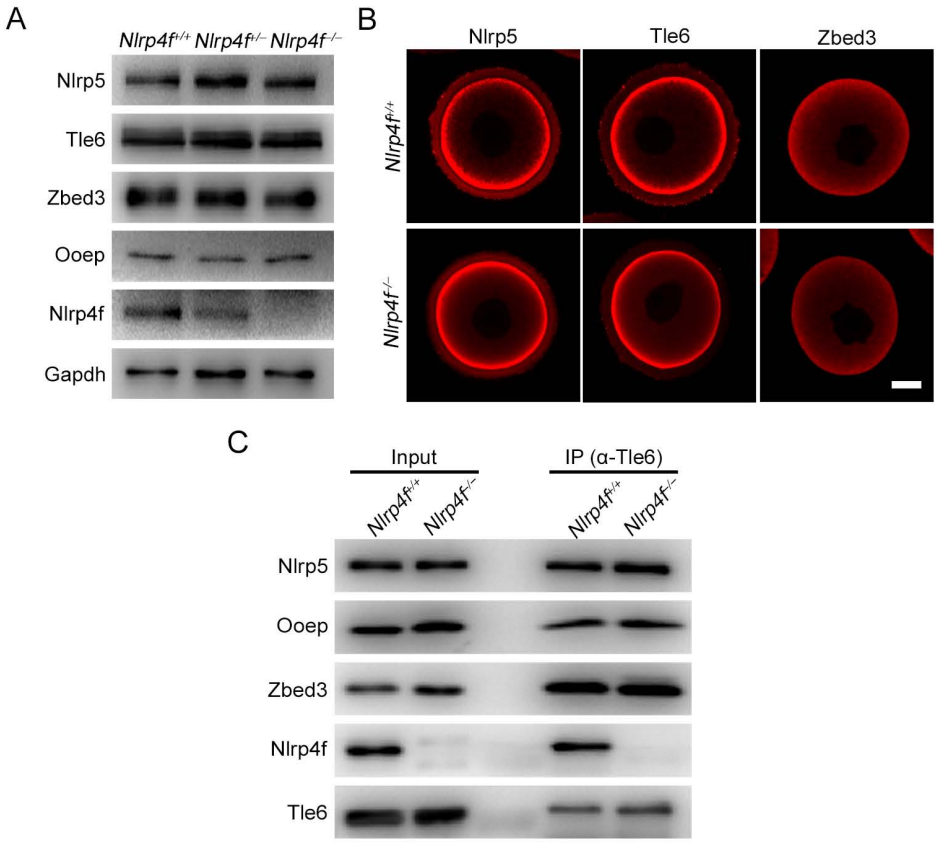

Figure S7. The expression patterns of the known SCMC components in *Nlrp4f*$^{-/-}$ oocytes. (A) Immunoblot of *Nlrp4f*$^{+/+}$, *Nlrp4f*$^{-/+}$ and *Nlrp4f*$^{-/-}$ GV oocytes with anti-Nlrp5, -Tle6, -Zbed3, -Ooep and -Nlrp4f antibodies. Gapdh was used as a loading control. (B) Immunofluorescent staining of GV oocytes from *Nlrp4f*$^{+/+}$ and *Nlrp4f*$^{-/-}$ females with anti-Nlrp5, -Tle6 and -Zbed3 antibodies. Scale bar: 20 μm. (C) Co-immunoprecipitation of GV oocytes (200) from *Nlrp4f*$^{+/+}$ and *Nlrp4f*$^{-/-}$ females with anti-Tle6 antibody, followed by immunoblot with specific antibodies for the SCMC proteins.

Figure S8

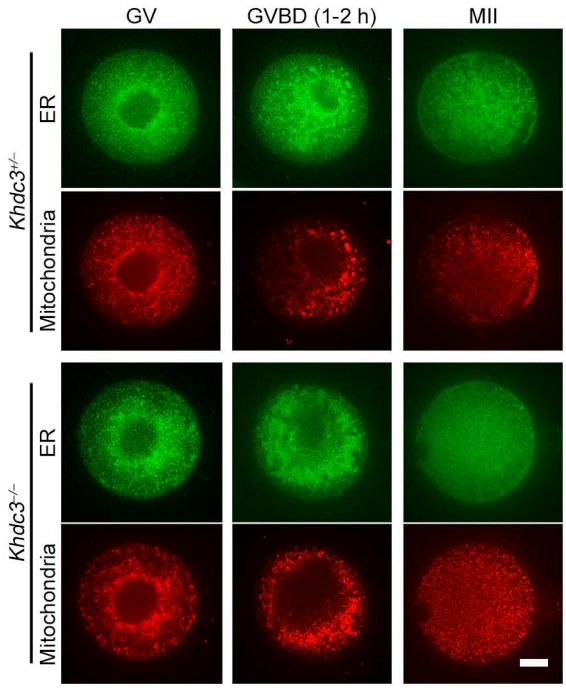

Figure S8. Disordered organelle distribution in *Khdc3*$^{-/-}$ oocytes. The oocytes were isolated from *Khdc3*$^{+/-}$ and *Khdc3*$^{-/-}$ females and were labeled with ER-Tracker (green) and MitoTracker (red) for ERs and mitochondria. *Khdc3*$^{-/+}$ (GV, n = 18; GVBD 1-2 h, n = 19; MII, n = 22) and *Khdc3*$^{-/-}$ (GV, n = 24; GVBD 1-2 h, n = 31; MII, n = 34) oocytes were investigated in three independent experiments. Scale bar: 20 μm.

Table 1 The list of antibodies

Primary antibodies			
Antibody	For immunoblot	For immunofluorescence	Source
Mouse anti-Nlrp5	1:1000	1:200	
Mouse anti-Tle6	1:1000	1:200	
Rabbit anti-Ooep	1:2000	-	
Rabbit anti-Zbed3	1:2000	1:200	
Sheep anti-Khdc3	1:500	-	
Rabbit anti-Nlrp4f	1:2000	1:200	Produced by Abmart
Mouse anti-Gapdh	1:5000	-	Sungene biotech, KM9002T
Mouse anti-β-actin	1:5000	-	Sungene biotech, KM9001T
Mouse anti-Acetylated-α-tubulin	1:1000	-	Abcam, ab24610
Rabbit anti-α-tubulin	1:1000	-	Cell signaling, 2144
Mouse anti-α-tubulin-FITC	-	1:200	Sigma, F2168

Secondary antibodies			
Antibody	For immunoblot	For immunofluorescence	Source
Alexa Fluor® 488 AffiniPure Donkey Anti-Rabbit IgG	-	1:500	Jackson Immuno Research, 711-545-152
Alexa Fluor® 594 AffiniPure Donkey Anti-Mouse IgG	-	1:500	Jackson Immuno Research, 715-585-150
Peroxidase AffiniPure Goat Anti-Rabbit IgG	1:5000	-	Jackson Immuno Research, 111-035-003
Peroxidase AffiniPure Goat Anti-Mouse IgG	1:5000	-	Jackson Immuno Research, 115-035-003
Peroxidase AffiniPure Donkey Anti-Sheep IgG	1:2000	-	Jackson Immuno Research, 713-035-003

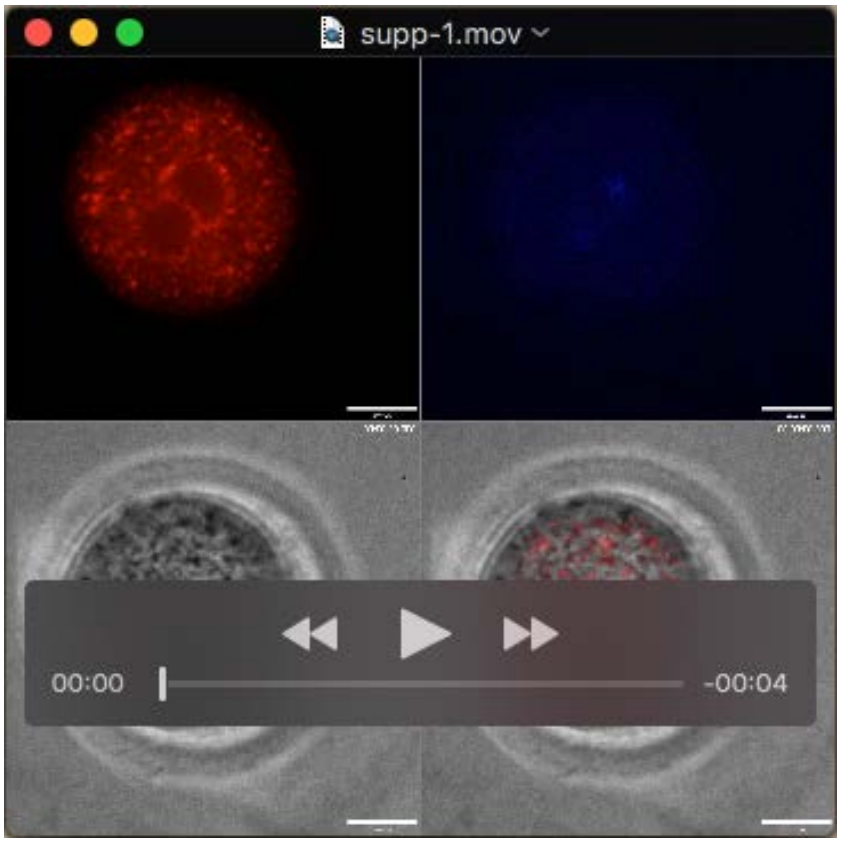

Movie 1. Mitochondria dynamics in the embryos from *Nlrp4f*$^{+/+}$ females during 1-cell to 2-cell development. Zygotes were isolated from *Nlrp4f*$^{+/+}$ females at 24 h after hCG stimulation, labeled with MitoTracker for mitochondria and Hochest 33342 for DNA and cultured to 2-cell stage. Time-lapse images were captured every 30 mins with UltraVIEW-VoX. Related to Fig. 4B.

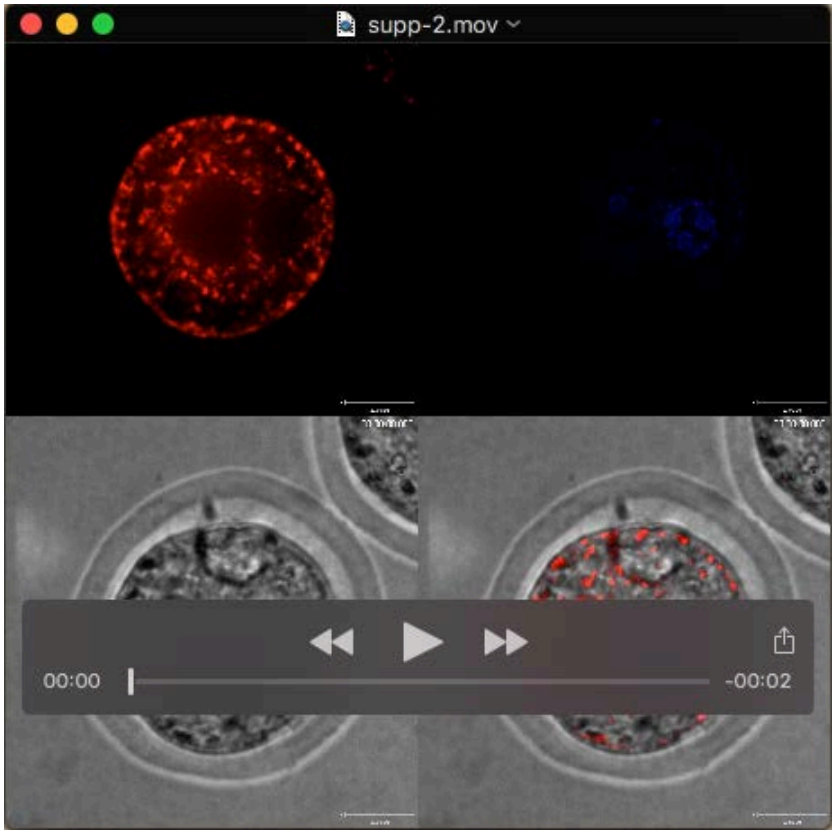

Movie 2. Mitochondria dynamics in the embryos from *Nlrp4f*$^{-/-}$ females during 1-cell to 2-cell development. Zygotes were isolated from *Nlrp4f*$^{-/-}$ females at 26 hrs after hCG stimulation, labeled with MitoTracker for mitochondria and Hochest 33342 for DNA and cultured to 2-cell stage. Time-lapse images were captured every 30 mins with UltraVIEW-VoX. Related to Fig. 4B.

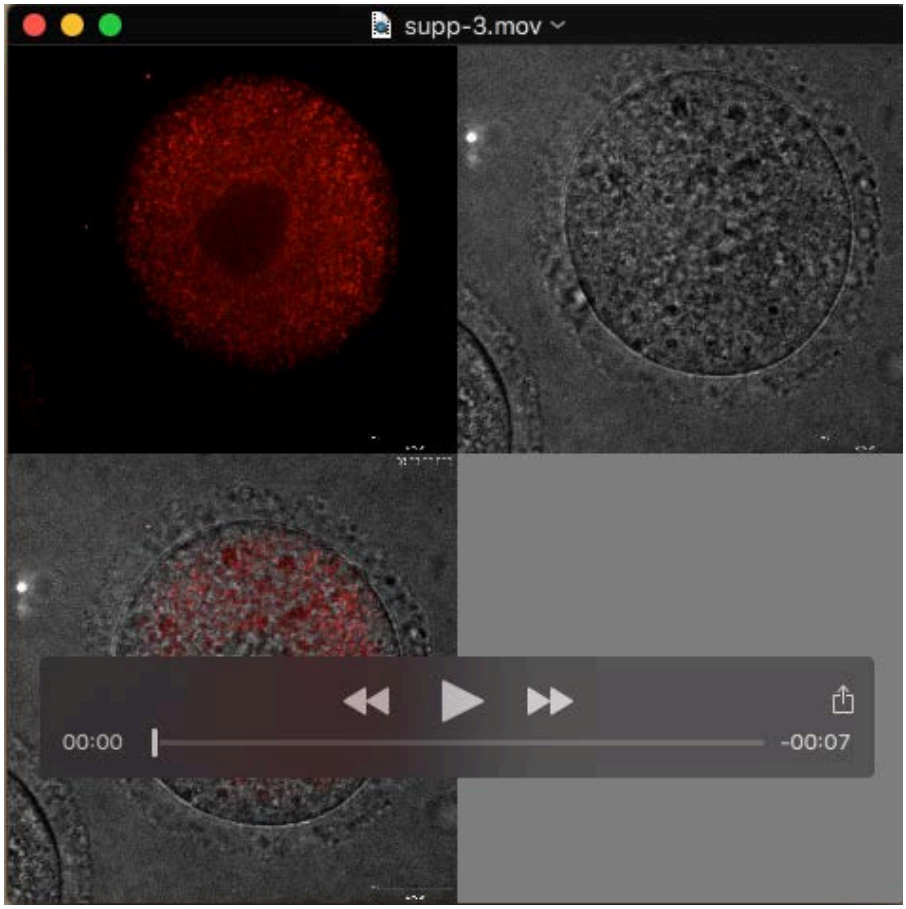

Movie 3. Mitochondria dynamics in the oocytes from *Nlrp4f*$^{+/+}$ females during GV to MII maturation. GV oocytes from *Nlrp4f*$^{+/+}$ females were labeled with MitoTracker for mitochondria and cultured to MII stage. Time-lapse images were captured every 30 mins with UltraVIEW-VoX. Related to Fig. 4D.

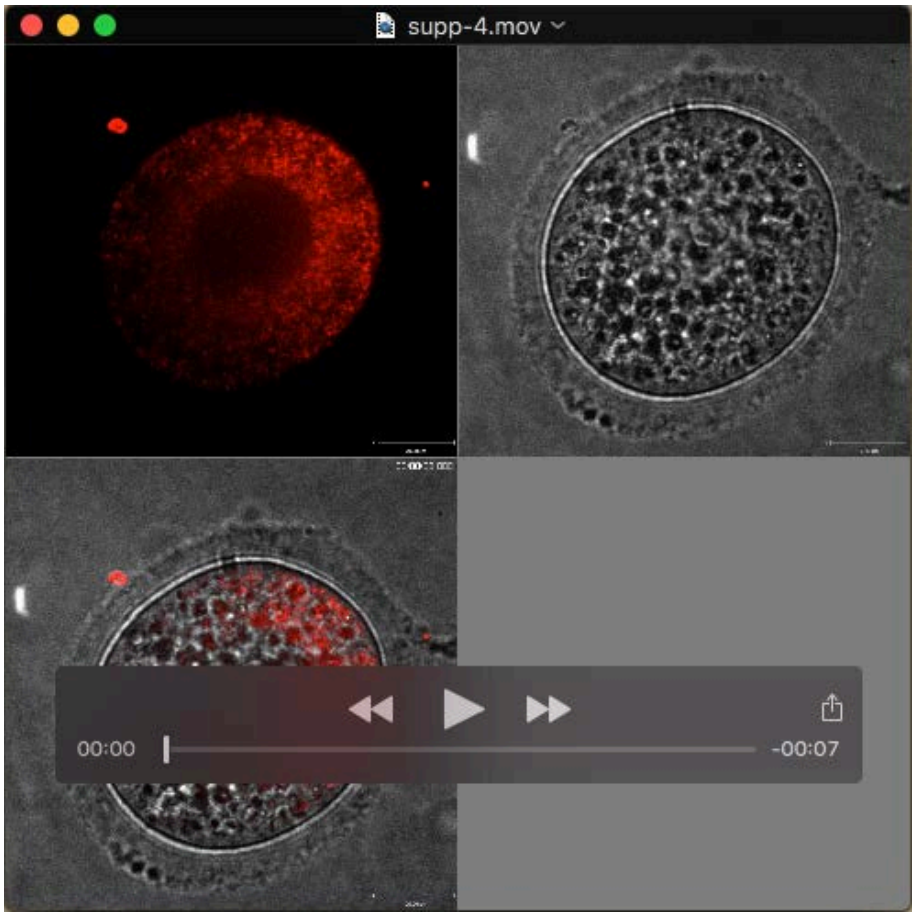

Movie 4. Mitochondria dynamics in the oocytes from *Nlrp4f*$^{-/-}$ females during GV to MII maturation. GV oocytes from *Nlrp4f*$^{-/-}$ females were labeled with MitoTracker for mitochondria and cultured to MII stage. Time-lapse images were captured every 30 mins with UltraVIEW-VoX. Related to Fig. 4D.